Todo list

AIX-MARSEILLE UNIVERSITY

DOCTORAL SCHOOL: Physics and Material Science

PARTENAIRES DE RECHERCHE

Laboratoire MADIREL

Submitted with the view of obtaining the degree of doctor

Discipline: Material Science
Specialty: Characterisation of porous materials

Paul Iacomi

Exploring sources of variability in metal organic frameworks through high throughput adsorption and calorimetic methods

Defended on 15/10/2018 in front of the following jury:

Rob Ameloot	KU Leuven	Rapporteur
Flor Siperstein	The University of Manchester	Rapporteur
Stefan Kaskel	TU Dresden	Examinateur
Jeff Kenvin	Micromeritics Inc.	Examinateur
Philip L. Llewellyn	CNRS/AMU	Directeur de thèse

National thesis number: 2017AIXM0001/001ED62

Abstract

Metal-organic frameworks (MOF) are a class of hybrid porous materials which has been the focus of much scientific interest since their discovery in the late 20th century. These coordination polymers consist of three-dimensional networks of metal nodes interlinked by polytopic organic molecules. The interest in these materials stems from the possible rational design of MOFs for highly efficient or unique applications. With judicious choice of building blocks, the framework can be used for carbon dioxide capture from air, hydrogen storage or regioselective catalysis. Taking advantage of specific properties of porous coordination polymers such as flexibility, magnetism or photoelectrics may even result in their use in drug delivery, micro mechanical devices, sensors or optoelectronics.

However, their unique properties also introduce significant difficulty in MOF characterisation through gas adsorption. Structural defects, crystal size, shaping procedure and the aforementioned flexible behaviour can lead to variability in adsorption results. In this thesis large scale processing of isotherms is first used to explore the scale of uncertainty present in porous material adsorption data. The high throughput methodology is then extended through the use of *in situ* calorimetry as an avenue to gain further insight into the contribution of material, guest-host and host-host interactions to the overall energetics of adsorption. Together, these two methods can be used to quantify the effect of structural defects in MOFs, material shaping with different binders and even yield fundamental know-how of how adsorption induces compliance in flexible materials.

Résumé

Les réseaux métallo-organiques (MOF) sont une classe de matériaux poreux hybrides qui ont suscité un grand intérêt scientifique depuis leur découverte à la fin du 20ème siècle. Ces polymères de coordination sont constitués de réseaux tridimensionnels de nœuds métalliques interconnectés par des molécules organiques polytopiques. L'intérêt pour ces matériaux provient de la conception rationnelle possible des MOF pour des applications hautement efficaces ou uniques. Avec un choix judicieux des blocs de construction, le cadre peut être utilisé pour la capture du dioxyde de carbone dans l'air, le stockage de l'hydrogène ou la catalyse régiosélective. Tirer parti des propriétés spécifiques des polymères de coordination poreux tels que la flexibilité, le magnétisme ou la photoélectrique peut même conduire à leur utilisation dans la délivrance de médicaments, des dispositifs micro-mécaniques, des capteurs ou en optoélectronique.

Cependant, leurs propriétés uniques introduisent également des difficultés importantes dans la caractérisation des MOF par adsorption de gaz. Les défauts structurels, la taille des cristaux, la procédure de mise en forme et le comportement flexible susmentionné peuvent entraîner une variabilité des résultats de l'adsorption. Dans cette thèse, le traitement à grande échelle des isothermes est d'abord utilisé pour explorer l'échelle d'incertitude présente dans les données d'adsorption des matériaux poreux. La méthodologie à haut débit est ensuite étendue à l'utilisation de la calorimétrie in situ comme moyen de mieux comprendre la contribution des interactions matériau-matériau, matériau-hôte et hôte-hôte à l'énergie globale de l'adsorption. Ensemble, ces deux méthodes peuvent être utilisées pour quantifier l'effet des défauts structurels dans les MOF, la mise en forme des matériaux avec différents liants et même un savoir-faire fondamental sur la manière dont l'adsorption induit la conformité dans les matériaux flexibles.

Acknowledgements

Contents

3. Exploring the impact of structural defects — post-synthesis generation of missing linkers in UiO-66(Zr)

3.1. Introduction

Ideality is a rarely encountered phenomenon in nature. In fact, experience has shown that deliberate and concerted efforts must be made in order to obtain states of matter that have all the properties described by an "ideal state". Often the divergence is small and can be approximated away, as is the case when using the ideal equation of state for of noble gasses or ascribing the thermal radiation emitted by an object to a black-body spectrum. It is, however, in non-ideality where the fascinating complexity of the world asserts itself and where advances in our understanding can be made.

When considering crystals, the ideal description of an infinite periodic repetition of building blocks in three dimensional space is not applicable in the real world. From the necessary existence of crystal boundaries to the possible presence of other structural irregularities, these so called crystal "defects" can have varying effects on the bulk properties of the material. Their presence is not necessarily a fault as they often impart the material with beneficial characteristics on multiple length scales. An understanding of the interplay of defects in the lattices of alloys is an art in itself. Crystal grain size and presence of additives such as carbon and nickel can completely change the hardness, ductility, tensile strength and corrosion resistance of steel.[1] Various other forms of disorder can introduce completely new behaviours altogether. The insertion of foreign elements into the crystal structure of semiconductor materials, such as silicon, can alter its electronic properties and is responsible for the ubiquitousness of computing devices based on the transistor.[2] This application of defects can be said to have ushered in the modern digital age, just as the creation of steel led to the industrial revolution. Other such emergent properties exist such as high temperature superconductivity[3] or thermoelectric behaviour[4] which are influenced by defect-related spin effects or defect-mediated charge transfer. As such, the kind of heterogeneity afforded by defects is a key attribute in condensed matter physics and a target for material design. The scientific foray in their control, either through generation or by inhibition can be termed "defect engineering".

As porous coordination polymers (PCPs) and their subclasses, metal organic frameworks (MOFs) and covalent organic frameworks (COFs), became prominent topics of study in the field of porous materials, the presence and desirability of defects in their ordered crystal structures has been put into question. Investigation of the propensity of these compounds to form defects has suggested potential benefits in the fields of catalysis [(5)], gas storage and separation [(6–8)], and has even alluded to applications in sensing and optoelectronics. [(9)] Furthermore, MOFs such as UiO-66 and similar oxo-Zr coordination compounds have been shown to have intrinsically defective structures, where clustering and correlation of defects is in fact inevitable. [(10)] The engineering of defects in PCPs is currently the focus of many initiatives as it is seen as a highly desirable method of tuning their properties through judicious design . [(5,11,12)]

From the point of view of describing adsorption in such materials, the presence of defects introduces a conundrum. If a MOF can be defective, and is often intrinsically so, a slight change in synthesis conditions can introduce a large variability in its properties, and obtaining a “standard” isotherm may be a challenge. A large scale meta analysis of the correlation between material structure and its adsorption performance cannot be achieved unless the contribution of defects is assessed for each material.

Chapter summary

In this chapter we explore the kind of changes in adsorption behaviour introduced through defect engineering with the high throughput processing tools presented in chapter 1. First, the range of crystal defects that can be found in MOFs is presented. A summary of the known methods for controlling defects in such materials is discussed, as well as the known impact on different properties. Particular focus is placed on the zirconium variant of UiO-66, due to its remarkable stability to the presence of defects in its structure. An alternative approach to defect generation in this MOF is explored, through induced leaching of linkers in a solvent solution of monotopic acids which have been shown to induce defect formation when present during synthesis. The influence on defect type and preponderence of the acid, its concentration and the solvent itself is investigated, through the changes in adsorption behaviour.

Contributions

This work was in done in collaboration with the DEFNET project partner at the Centre for Surface Chemistry and Catalysis in KU Leuven. The study was designed by Paul Iacomi and João Marreiros during the secondment undertaken in COK as part of this project. Two PWI master students, Giel Arnauts and Wouter Arts helped with the synthesis, leaching and characterisation of the first trial batch. João Marreiros conducted the synthesis, leaching, XRD and NMR of further batches in Leuven. Paul Iacomi performed characterisation through TGA and all physisorption measurements in Marseille. Prof. Philip Llewellyn and Prof. Rob Ameloot provided critical input in the direction of the study and the significance of the results.

3.2. The defective nature of MOFs

3.2.1. Types of crystal defects and their analogues in MOFs

From a crystallographic point of view, defects can be described as features which suspend the order of components in an ideally regular lattice. The building blocks in the case of MOFs can be either individual atoms, molecules or other higher order structure building units (SBUs). Any change with leads to local breaking of symmetry with respect to that original structure can be viewed as a defect.

With respect to dimensionality, defects can be described as point defects, line defects (such as edge dislocations), plane defects (such as grain boundaries or stacking faults) and bulk defects (macroscopic voids, phase coexistence). When it comes to point defects, we can broadly refer to several types: **substitutional defects**, where an existing building unit is replaced or transformed into another, **inclusion** or **interstitial defects**, where a foreign component or building block is included in the framework and **vacancy defects** where one of the lattice sites is unoccupied. In the context of MOFs, the same general categories of defects apply. However, due to the higher degrees of freedom available in these compounds, a greater variety of potential crystal defects can exist.

Vacancy defects are encountered through missing linker and missing cluster defects. These analogues to Schottky defects arise from the removal of one or several topological nodes or vertices. In most cases, the charge neutrality of the framework is maintained through coordination of available counterions or solvent molecules, though changes in the oxidation state of the metal atoms may also occur.

Substitution point defects are also highly common in MOFs, as the usual requirement for framework connectivity is the existence of "click groups" on metal nodes and linkers. Any molecule which fulfils the connectivity and size requirements may be used, a property which has been exploited in the topological approach to creating new MOFs.[13–15] It also allows for MOFs in which nodes or vertices are only partly replaced with analogues to be created. This strategy has been successfully employed to create mixed-linker or mixed-metal structures.[16,17] It should be noted that if the distribution of the substitutions takes a homogenous pattern throughout the lattice, the structure may no longer fall under the definition of a defect.

A special case of substitutional defects which are present in MOFs are mixed valence defects. When metals with multiple stable oxidation states, such as Cu (I – II), Fe (II – III) etc. are part of the framework, a change in their oxidation state can occur. This has been shown to be

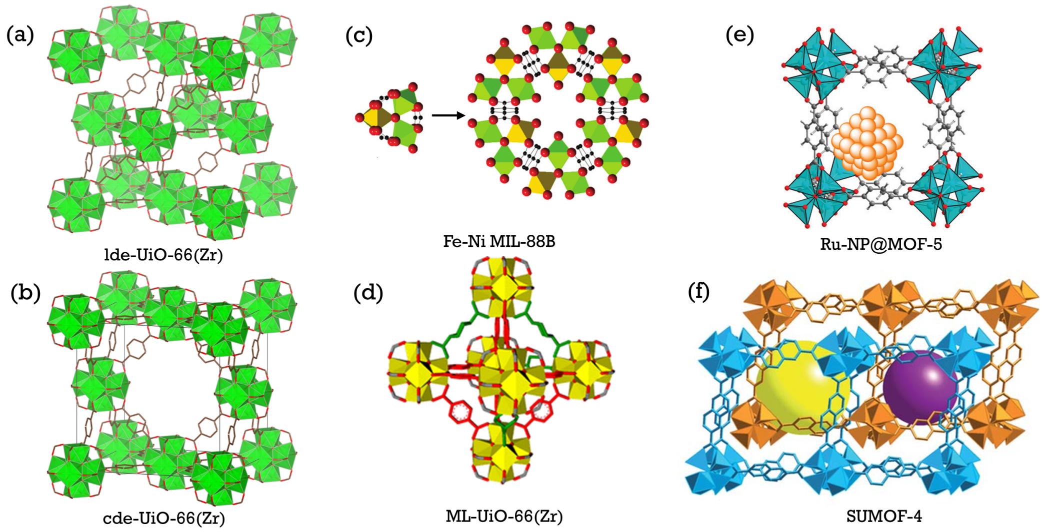

Figure 3.1.: Different types of defects as seen in MOFs: vacancy defects in the form of (a) missing linker and (b) missing cluster substitutional defects such as (c) mixed linker (16) and (d) mixed metal (22) MOFs or defects as created through (e) nanoparticles (21) or (f) interpenetration (23)

an integral part of copper paddlewheel and iron trimesate containing MOFs (18) and can even be seen with the naked eye, as such defects have been shown to give HKUST-1 its common blue colour. (19)

Inclusion-type point defects are loosely applied to MOFs. As the definition describes an interstitial defect to be an atom occupying an usually vacant space, all foreign bodies occupying the available porosity of the MOF, including aforementioned counterions and solvents could be considered as defects in the traditional crystallographic sense. Introduction of nanoparticles such as metals or metal oxides inside the pores is a more traditional view of such defects. These have been shown to have beneficial effects in catalytical applications. (20,21)

A common feature of structured high porosity compounds is interpenetration. While not a defect in the classical sense, it has important effects on their properties. (24) With a large enough pore size, a secondary lattice can form in the pore voids of the primary one. This imposes a limit on the common design strategy of isoreticular synthesis, but can introduce new features such as better adsorption through confinement, increase in active site count and even flexibility.

Finally, the surface of the MOF can also be regarded as a boundary or plane defect. The nature of the surface plays a role in intra-particle interactions, important when considering the agglomeration behaviour or inclusion of crystals in a membrane. (25) The surface properties play a crucial role in MOFs which are synthesised as thin films (26,27), where the nearly 2D materials are better defined by interfacial characteristics than through bulk properties. Crystal size effects on MOF properties such as flexibility can also be through of as a consequence of surface characteristics, more specifically of surface-to-volume ratio. When considering such soft materials [28,29], it has been shown that the flexible behaviour is highly influenced by entropy barriers introduced by the surface.

3.2.2. Consequences of defects

The introduction of defects in the regular crystal lattice of metal organic frameworks can have a dramatic impact on their properties. In general, the following may occur:

- the porosity of the structured is altered, increasing in the case of vacancy defects and decreasing when bulky substitutions or inclusions are made;
- interactions with adsorbed molecules change, through the different pore environment encountered or through the generation of coordinatively unsaturated sites (CUS);
- the stability of the resulting structure is lower than that of the parent MOF, influencing bulk mechanical and thermal properties.
- electronic properties can be changed which may affect the optical electric or magnetic behaviour of the material.

From a purely geometric point of view, the introduction of missing linker or missing cluster defects leads to more voids in the structure, increasing its porosity. It often results in a larger specific surface area and pore volume and thus useful for applications such as gas storage which depend only on the available surface or capacity. Macro-scale void networks can also be desirable, as the better developed pore network has a large impact on the transport properties of the compound, increasing diffusion rates.

The inclusion of defects also changes the landscape of the pore walls leading to different interactions with adsorbed molecules. Charge balancing counterions, molecules capping defect sites, functionalisations of substituted linkers or CUS can change the chemistry of the pore, with specific interactions towards certain adsorbates. [30] For example, adsorption of water on oxo-Zr MOFs, has been seen to be dominated by the percentage of defects. The pore filling step can shift from high partial pressure (0.6 p/p_0) to much lower pressures as seen in UiO-66 [7] and MOF-801. [6] Defect site adsorbed molecules can also lead to cooperative phenomena, such as the beneficial effect of defect-adsorbed water on the catalysis of Fischer esterification. [31] or the CO_2 capture on amine-grafted metal centers. [32] Another example can be seen in MOFs containing Fe trimers, such as MIL-127(Fe) or MIL-100(Fe) where heating or acid treatment can induce a reduction of one of the iron atoms, generating additional Lewis sites for catalysis [18] or providing CUS for cooperative binding of carbon monoxide through a spin transition mechanism. [33]

Of course, defects are also problematic. Most metal organic frameworks synthesised to date suffer from poor stability. Even if the material is crystalline when solvated, the framework may not have enough structural stability to be able to sustain itself when fully evacuated. The activation process itself can lead to framework collapse, due to the forces encountered in guest removal, necessitating complex activation processes, such as supercritical drying or preliminary solvent exchange. After activation, the metal-ligand bond is susceptible to attack by adsorbed species. Here, defects in the framework have been shown to play a major role in its stability (or lack thereof).[(34)] Copper paddlewheel containing structures are particularly vulnerable to such attack.[(35)]

Finally, several completely different phenomena may emerge through the introduction of defects. Optical properties such as colour centers and induced luminescence[(19)], changes in thermal conductivity or induced magnetic properties such as ferromagnetism[(36)] have been shown to be a consequence of the presence of defects.

3.2.3. Defect engineering of MOFs

Since defects introduce another degree of freedom for controlling the properties of metal organic frameworks, the study of their formation can lead to new methods of tuning a material towards a desired application. There are two major pathways of introducing defects, through control of the structure during synthesis or through post-synthetic methods.[(37)]

For defect generation during synthesis, the so called "solid solution" approach is to mix several types of building blocks together, be it multiple linkers or metallic nodes. Mixing functionalised versions of linkers leads to the creation of partially-substituted MOFs. Mixed valency frameworks can also be synthesised through this method, as can be seen in the replacement of up to 32% of the linker in the framework in the ruthenium HKUST-1 analogue with a defect-generating linker.[(38)] The commonly used method of improving crystalinity and particle size of modulator-assisted synthesis[(39)] has been shown by Shearer et al. to be a reliable method of introducing defects.[(40)] The modulators act as capping agents and occupy metal coordination sites.

Post-synthetic methods are also widely employed for defect generation. Through acid treatment of the previously mentioned MIL-100(Fe), cleavage of one of the Fe–O bonds can be induced, with a protonation of the carboxylic linker and the generation of a CUS.[(41)] Thermal treatment can achieve the same results, with weakly coordinated molecules removed to expose metal CUS or even *in situ* linker decomposition.[(42)] Ligand exchange has also been shown to be achievable post-synthetically, [(43)] through the replacement of existing linkers, capping agents or even induce structural "healing". Finally, the linkers are still available for organic reactions which can transform a part of them into functionalised versions, as seen in the nitration of the terephtalate linker in MIL-101.[(44)]

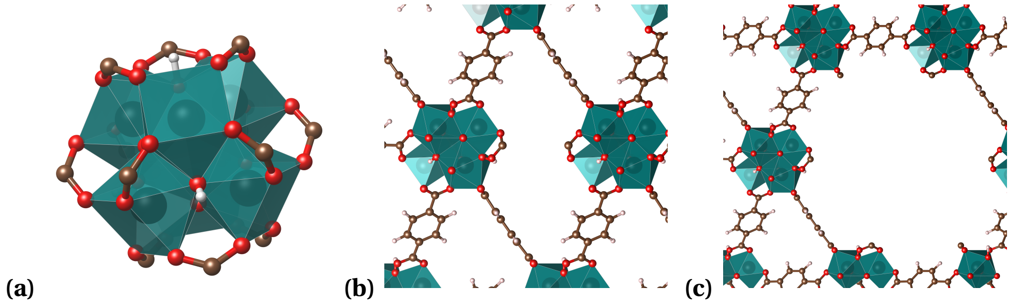

Figure 3.2.: (a) The 12-coordinated Zr cluster in UiO-66(Zr) which connects with benzene dicarboxilate (BDC) linkers. Two prototypical defect types are shown (b) a missing linker defect and (c) a missing cluster defect. Zirconium octahedra are represented in turquoise, oxygen in red, carbon in brown and hydrogen in white.

3.2.4. The propensity of UiO-66(Zr) for defect generation

The UiO-66(Zr) MOF and its derivatives are well known due to their thermal and chemical stability.[45] It is composed of $[Zr_6O_4(OH)_4]^{12+}$ clusters (seen in Figure 3.2a) which are connected via benzene dicarboxilate (BDC) linkers to form a face-centred cubic framework. Due to its exceptional stability among MOFs, it has been the focus of much research, where it has shown promise[46] in use for gas adsorption and catalytic applications.

The synthesis of many functional derivatives of UiO-66, through the use of different struts of nodes has been a stepping stone towards obtaining mixed-linker and mixed-metal materials, either thorough the solid solution or post-synthesis modification approach.[47] It has also been used as a support for nanoparticles, such as palladium[48] or platinum.[49]

However, UiO-66 is particularly adept is in its ability to support vacancy defects. Due to the stability of the metal-oxygen bond, and the high linker to metal ratio, the UiO family of MOFs can tolerate a high degree of defectivity in their structure, which manifests through either missing linker (Figure 3.2b) or missing cluster (Figure 3.2c) defects. Ever since the discovery of a number of defects in the pristine material through neutron powder diffraction methods[50] and the theoretical basis laid down by Cliffe et al.[10] for the existence of correlated defective nanodomains where the existence of a vacancy induces defect formation in neighbouring sites, this MOF became a prototypical framework for the study of such defects. The modulated synthesis approach, initially used as a means of creating novel topologies and controlling crystal size[51] has been remarkably successful in obtaining defective versions of UiO-66(Zr).[40] Post-synthetic methods such as ligand exchange[43], temperature-induced dehydroxilation of the zirconium cluster[52] and thermal removal of one of the linkers in a mixed-linker variant[16] have been similarly adept in obtaining voids in the structure. More recently, the interplay between the defective nature of UiO-66 and the mechanism of post-synthesis linker exchange[53] has been put into the limelight.

In these defects, the metal sites are almost always capped, with monoacids such as formate and acetate, water, hydroxyl groups or other counterions being able to assume the role of capping agent. It has been shown by Thornton et al. that the influence of such defects on the adsorption properties depend not only on their position, but also on these capping agents. [54]

Such vacancy defects prove to be useful for generating Lewis sites for catalytic application, as can be seen in the 4-fold increase in conversion in citronellar cyclization or the increase in 4-tert-butylcyclohexanone reduction from 5–7% to almost 90%. [55] They are also useful for gas separation, as they can increase the interaction towards a component of the mixture, seen for example on the increased efficiency of CO_2 / N_2 separation. [54]

It can therefore be concluded that vacancy defects are a fundamental characteristic of this MOF, with wide-ranging effects in its properties. As such, it is desirable to have methods to generate and control them. In the following pages, we examine a tertiary method for vacancy defect generation: leaching in solvent solution, a method which has been previously shown to be applicable to other MOFs. [56]

3.3. Materials and methods

3.3.1. Materials

The UiO-66(Zr) MOF used in this study was synthesised according to the procedure described in section B.4, which was adapted from Shearer et al. [57]. This particular method was chosen to ensure that a structure with a minimal number of intrinsic defects would be obtained.

The resulting parent MOF was activated for 8 h at 200 °C to ensure that all solvent was removed. 200 mg aliquots of material were prepared and placed in vials, alongside the monotopic acid dissolved in 20 ml of the respective solvent. The quantities of acid correspond to molar quantities of the framework. The samples were then gestated over a 24 h period at 80 °C in a temperature controlled oven. Pressure resistant Schott sealed bottles were used to ensure that solvents with a lower boiling point do not evaporate. After leaching, samples were collected and washed in ethanol for 4 h, a procedure repeated 4 times. Finally, all samples were dried at 120 °C.

To generate a comprehensive map of the influence of different variables on defect concentration, a number of leaching conditions have been selected. The same monotopic acids which have been successfully used as modulators in the synthesis of defective UiO-66 (formic acid (FA), acetic acid (AA), trifluoroacetic acid (TFA) and benzoic acid (BA)) were used in various concentration ranges, from 1 to 100 molar equivalents with respect to the framework. In order to verify the contribution of the solvent N,N'-dimethylformamide (DMF), deionized water, ethanol and dimethyl sulfoxide (DMSO) were used as the leaching medium. Two parent materials have been synthesised, PWI-C which formed the basis of the initial DMF test trial, and JM237 which was made in bulk to be used for subsequent solvent batches. The DMF dataset does not include any trifluoroacetic acid leached samples, as it was only used in the latter sample sets. Furthermore, no benzoic acid samples could be generated when using water as a solvent, due to its poor solubility. Finally, at high acid concentrations, several of the samples were completely dissolved during leaching conditions. The mass loss during leaching was found to be between 10 and 60%, depending on the acid and solvent used. When using 10 equivalents of TFA in DMSO, only 18% of the original sample could be recovered. A summary of all generated materials can be found in Table 3.1. Some properties of the acids and solvents used, such as acidity, solubility, etc. are found in Table E.2 and Table E.1 in Appendix E respectively.

3.3.2. Methods for quantifying defects

Determining the abundance of missing linker and missing cluster defects and characterising their distribution is a major challenge, as the components of the framework to not change, only their local order.

If the distribution of defects can introduce changes in the long-range order and topology of their parent framework, such as by the introduction of phase changes, additional peaks can be observed through regular powder diffraction techniques. As Cliffe et al. [(10)] has shown, the UiO-66 defect-free face-centred unit (**fcu**) net can be transformed through missing cluster defects into a (**reo**) net. Short-range correlations of such domains form nanoregions inside the parent structure and generate diffuse scattering peaks observable at low angles in powder X-ray (pXRD) diffraction patterns, corresponding to "forbidden" reflections in a primitive cubic superstructure. As such, these pXRD peaks can be used to verify the existence of missing cluster defects, but only when their abundance allows for nanodomains of (**reo**) nets to be formed. In this study, pXRD measurements were performed as described in section A.8 as quick screening for a large degree of defectivity.

One of the most accessible way of assessing the defectivity of a MOF is thermogravimetry (TGA). Through heating in an oxygen-rich atmosphere, the MOF is normally reduced to its metal oxide and a stoichiometric analysis of the TGA curve can allow for the percentage of missing linkers to be determined. TGA curves for this study were measured under an air atmosphere using the method described in section A.1. A heating rate of 5 °C min^{-1} was used. The curves are then normalized with respect to the weight at 600 °C, which corresponds to pure ZrO_2. The maximum possible mass loss of a solvent-free structure is calculated from the ratio of the fully-substituted, but dehydroxilated, metallic cluster $Zr_6O_6(C_6H_4(COO)_2)_6$. The plateau of the TGA curve between 400 °C to 500 °C, in the range where it is assumed that the molecules included in the framework are completely evacuated, is used as a measure of the number of terephtalate linkers which are missing.

Table 3.1.: Samples used in the UiO-66(Zr) linker leaching study

Sample name	Solvent	Modulator	Concentration	Observations
PWI-C	None	None	None	Parent material
FA1	DMF	FA	1:1	—
FA5	DMF	FA	1:5	—
FA10	DMF	FA	1:10	—
FA20	DMF	FA	1:20	—
FA100	DMF	FA	1:100	—
AA1	DMF	AA	1:1	—
AA5	DMF	AA	1:5	—
AA10	DMF	AA	1:10	—
AA20	DMF	AA	1:20	—
AA100	DMF	AA	1:100	—
BA1	DMF	BA	1:1	—
BA5	DMF	BA	1:5	—
BA10	DMF	BA	1:10	—
BA20	DMF	BA	1:20	—
BA100	DMF	BA	1:100	Completely dissolved
JM237	None	None	None	Parent material
JM328	H_2O	FA	1:10	—
JM329	H_2O	FA	1:100	—
JM330	H_2O	AA	1:10	—
JM331	H_2O	AA	1:100	—
JM332	H_2O	BA	1:10	—
JM333	H_2O	BA	1:100	—
JM334	H_2O	TFA	1:10	—
JM335	H_2O	TFA	1:100	—
JM351	MeOH	FA	1:10	—
JM352	MeOH	FA	1:100	—
JM353	MeOH	AA	1:10	—
JM354	MeOH	AA	1:100	—
JM355	MeOH	BA	1:10	—
JM356	MeOH	BA	1:100	—
JM357	MeOH	TFA	1:10	—
JM358	MeOH	TFA	1:100	—
JM359	MeOH	None	0	Control
JM360	DMSO	FA	1:10	—
JM361	DMSO	FA	1:100	—
JM362	DMSO	AA	1:10	—
JM363	DMSO	AA	1:100	—
JM364	DMSO	BA	1:10	—
JM365	DMSO	BA	1:100	—
JM366	DMSO	TFA	1:10	—
JM367	DMSO	TFA	1:100	Completely dissolved
JM368	DMSO	None	0	Control

In order to check for the inclusion of a modulator in the framework, the MOF can be digested with the help of a hydrofluoric acid and the resulting solution can be analysed through proton nuclear magnetic resonance (^{1}H NMR) or high performance liquid chromatography (HPLC). In this study, ^{1}H NMR was used through the procedure detailed in section A.9 to qualitatively and quantitatively assess the presence of the capping agents in the UiO-66(Zr) samples.

Finally, both nitrogen adsorption at 77 K and CO_2 adsorption at 303 K can be used to describe the surface characteristics and porosity of the samples. The methods for obtaining the isotherms are presented in detail in section A.4 and section A.7 for N_2 and CO_2 respectively.

3.4. Results and discussion

3.4.1. Crystalinity of leached samples

The crystalinity of the leached samples is verified through XRD. The results in section E.2 confirm that all resulting materials retain the same peaks in their powder diffraction patterns.

A closer look at the low angle scattering (Figure 3.3) reveals the appearance of diffuse peaks, which are marked in the figure by black arrows, which correspond to forbidden reflections of the (**reo**) phase. They confirm that the leached samples begin to exhibit phase coexistence of the original UiO-66(Zr) unit cell and the missing cluster (**reo**) net. These peaks have the highest intensity in the TFA treated materials, suggesting that it has the highest capability of introducing missing cluster defects.

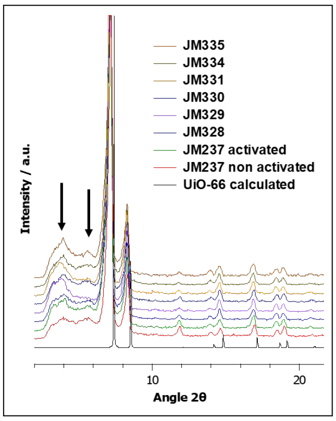

Figure 3.3.: Diffuse scattering peaks in the H_2O leached samples, highlighted by black arrows.

3.4.2. Thermogravimetry results

A typical TGA curve, as measured on a pristine material is characterised by three main mass losses: a loss at low temperature, usually until 100 °C, which is indicative of adsorbed water from the environment; a secondary mass loss in the 100 °C to 200 °C range, corresponding to the evacuation of residual solvent from the pores and finally, a large step which is a sign of sample degradation as the linker is oxidized.

A selection of TGA curves measured on the leached samples can be seen in Figure 3.4. The complete set of data can be found in Appendix E, section E.3.

There are four types of differences that can be arise between curves on different samples:

- the aforementioned change in overall height, which indicates the presence of missing

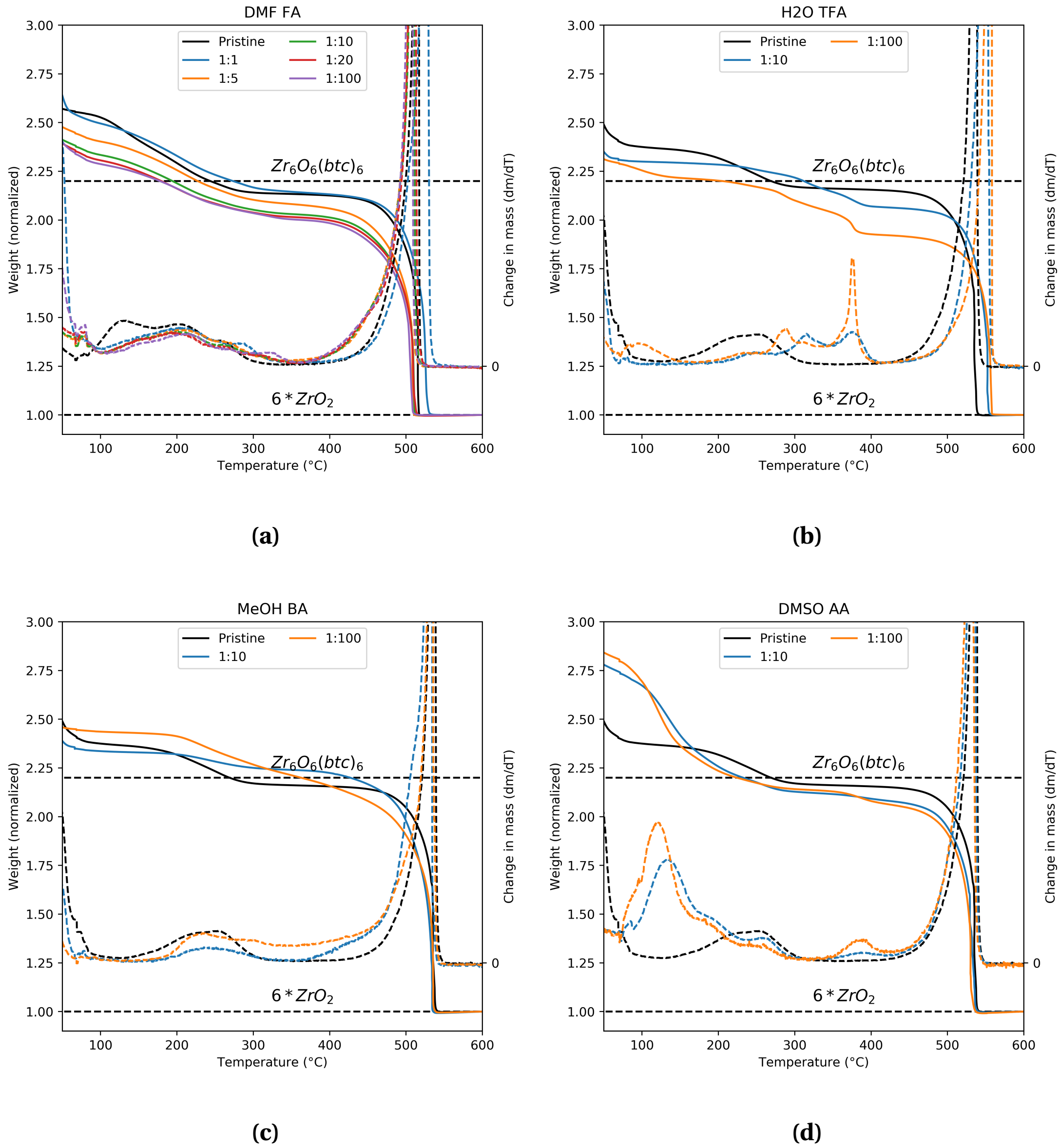

Figure 3.4.: A selection of the TGA curves as measured on the leached samples: (a) formic acid in DMF, (b) trifluoroacetic acid in water, (c) benzoic acid in methanol and (d) acetic acid in DMSO. The curve for the parent material is in black. Dotted lines correspond to the secondary y axis as a semilogarithm of the first derivative of mass loss with respect to temperature.

linker defects;

- differences in the solvent removal step, as they have different boiling points and interactions with the framework;
- in case the defects are capped by an agent such as the modulator molecule used, it may introduce a new mass loss step between solvent removal and complete structure breakdown;
- finally, a highly defective structure loses part of its thermal resistance altering both the onset of mass loss and the final decomposition temperature.

From the TGA curve of the pristine UiO-66 material, it is immediately obvious that there are some defects already present in the sample. By using the normalized mass at 420 °C a linker-to-cluster ratio of around 11.6:1 can be calculated. This shows that there are still intrinsic defects in the as-synthesised structure. These defects are most likely capped by formate moieties, which have been generated during the solvothermal synthesis in DMF through solvent self-hydrolysis (Equation 3.1), as commercially available solvent has a small percentage of residual water.[40]

$$HCON(CH_3)_2 + H_2O \longrightarrow HCOOH + HN(CH_3)_2 \tag{3.1}$$

It follows that the mass loss step around 250 °C is the evacuation of formate capping agents from the structure, to generate an open metal site. The same step can be found in the samples which have been leached with formic acid.

In leached samples where other acids were used, it is likely that the original formate capping the defects has been replaced with an acid molecule from solution, either because it is thermodynamically favourable, or simply through kinetic means due to the large excess present. As evidenced in Figure 3.4, the mass loss corresponding to the formate is reduced, or no longer seen. Acetic acid (Figure 3.4d) leaves the structure at a higher temperature, as a new peak is present at 390 °C. Strongly bound capping agents at defect sites have been shown to require a higher activation temperatures to be fully removed.[58] Benzoic acid (Figure 3.4c) introduces a progressive mass loss near the total decomposition temperature of 550 °C. As it is similar to the BTC linker, its higher stability is not surprising. Finally, the samples leached with TFA have a more complicated curve, with two or even three peaks in the first derivative with respect to temperature. This kind of degradation suggests the existence of different types of capping sites, some more strongly bound than others. A slight difference is also observed in their thermal stability, with all TFA samples having a 20 °C to 30 °C increase in decomposition temperature. Since defects normally have a negative impact on the thermal and mechanical resistance of a MOF, high resolution TGA experiments were carried out to eliminate possible influences of heating rate. The resulting curves (Figure E.5) still display the same behaviour. The effect is likely due to the electron-withdrawing effect of the TFA molecule on the Zr node, which induces a stronger Zr-carboxilate bond. A similar paradoxical increase in mechanical stability has been shown by Van de Voorde et al.[59] on TFA modulated defective UiO-66 materials.

The solvent used can be removed in all cases before 200 °C. DMSO has the highest preponderence in the leached samples (Figure 3.4d) and is the most difficult to remove, likely due to its higher boiling point.

It is also clearly visible that the leaching procedure led to the generation of defects. The curves of the leached samples fall below that of the original material in normalized weight, indicative of a lower linker-to-node ratio. These trends are analysed in subsection 3.4.4.

3.4.3. Nitrogen sorption at 77K

Isotherms have been recorded on samples activated at both 200 °C and 320 °C. It is important to note that, as seen from the TGA curves, not all capping agents leave the structure when thermally treating at a lower temperature. The moieties which are still coordinated to the Zr cluster will likely influence the adsorption behaviour. At a high temperature, the dehydroxilation of the metal center also occurs[52], which may also affect the interaction with physisorbed probes. Several example isotherms can be found in Figure 3.5, with the complete dataset present in Appendix E, section E.4.

There are a few isotherm features which can be analysed to assess the type of modifications introduced in the structure and their preponderence.

- The slope of the isotherm at low p/p_0 is representative of the first interactions with the pore surface, which can be quantified using the initial Henry constant. It will be influenced by any changes in pore environment such as CUS or functionalised defect sites.
- Missing liker defects will lead to an increase of the apparent surface area and perhaps to a more extensive pore network.
- The pore size distribution and total pore volume give indications on the presence of missing cluster defects and/or of the formation of mesoporous voids within the structure.
- A steep step at high p/p_0 is indicative of intercrystal condensation and suggests particle aggregation due to lower average crystal size.

It is immediately apparent that the leaching process had an influence on the adsorption characteristics of UiO-66. Isotherms of acid treated samples diverge from the parent material, often at different pressures. In general, the total molar capacity at full loading is seen to increase, a telltale sign of an increase in pore volume through defect generation. On the other hand, other particularities exist, such as the benzoic acid samples in methanol and DMSO

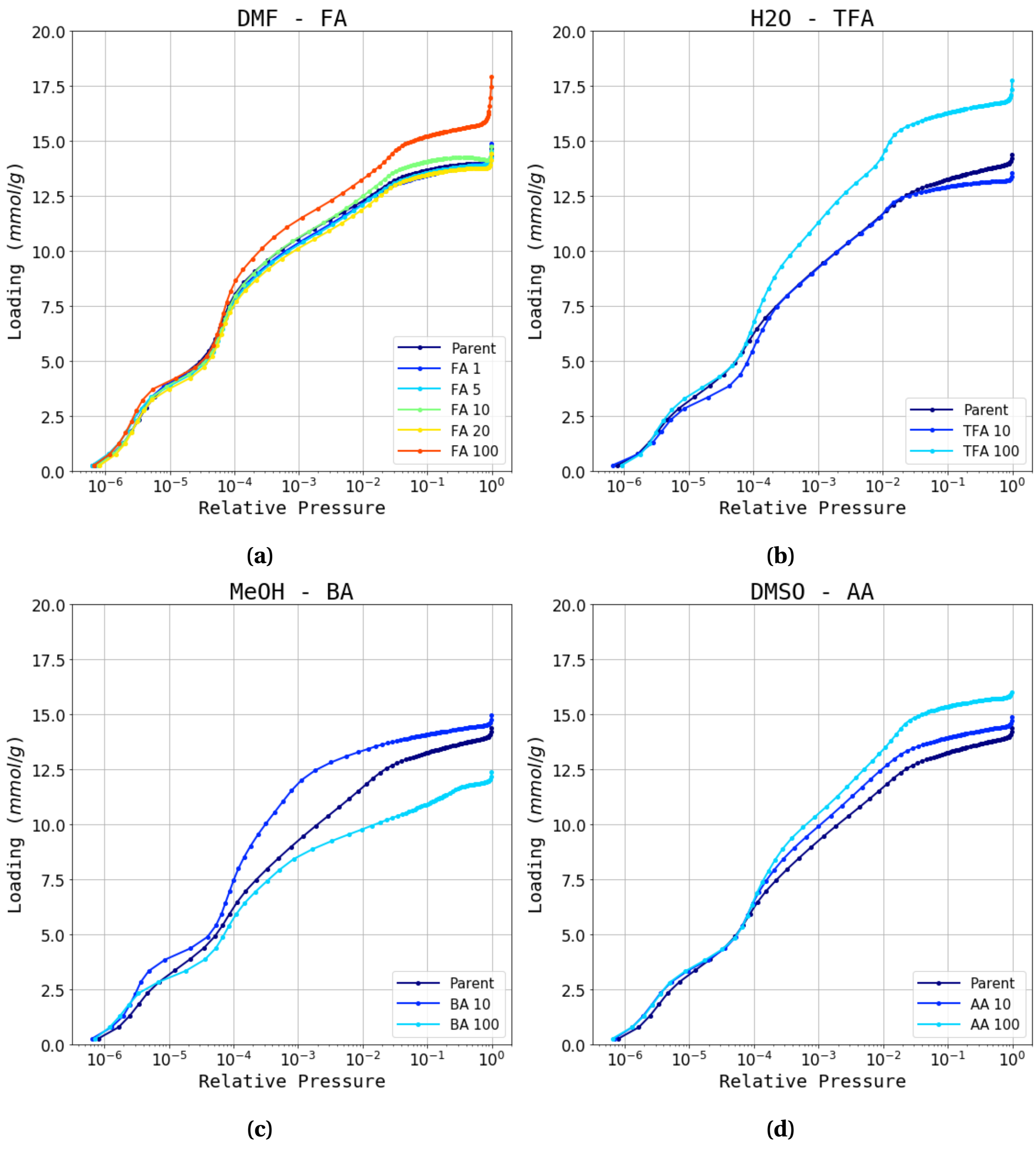

Figure 3.5.: A selection of nitrogen sorption isotherms as measured on the leached samples at 200 °C: (a) formic acid in DMF, (b) trifluoroacetic acid in water, (c) benzoic acid in methanol and (d) acetic acid in DMSO. The curve for the parent material is in dark blue. The x axis is logarithmic for clarity of low pressure points.

where the low and high concentration has opposite effect on the total loading. Predictors of defects and trends will be analysed in the following section.

3.4.4. Characterisation of trends

The graphs in Figure 3.6 summarize the trends in missing linker defects as calculated through the TGA plateau at 420 °C. The DMF leached samples, due to the multiple datapoints with different acid concentrations show the clearest influence of this variable on defect generation. Even small amounts of modulator lead to the decrease of the linker-to-node ratio, but the increase in concentration stops having an effect at around 20:1 equivalents. It is likely that the trends are similar with other solvents, even if less datapoints are available.

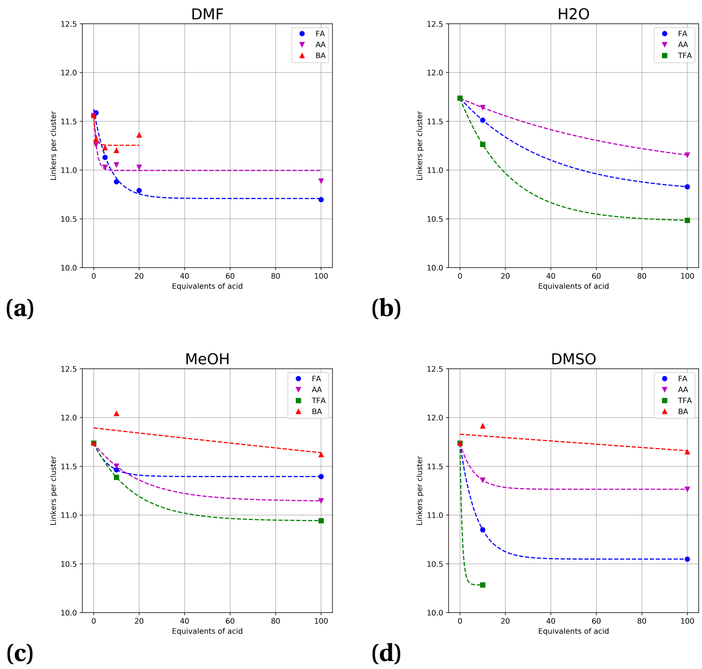

Figure 3.6.: Calculated linker-to-node ratio from the TGA curve normalized mass at 420 °C for (a) DMF (b) H_2O, (c) MeOH and (d) DMSO leached samples. A ratio of 12 to 1 corresponds to a completely defect-free structure. An exponential decay trendline is fitted to each set of points.

In the case of benzoic acid the data bears careful interpretation. Thermogravimetric methods may not be suitable for assessing the resulting defects. The comparatively large molecule, high boiling point and similarity to the terephtalate linker make the removal of benzoic acid capping open metal sites harder, and as such, the plateau is not an accurate indication of defectivity. Indeed, the calculated linker ratio is seen to actually increase in the case of methanol and DMSO. It is here proposed that in benzoic acid leached samples defect generation occurs through the coordination of two benzoic molecules (or one, in the case of a "dangling" linker), as seen in Figure 3.7, with the increased amount of organic material effectively compensating for any defects that could be seen in the TGA curve.

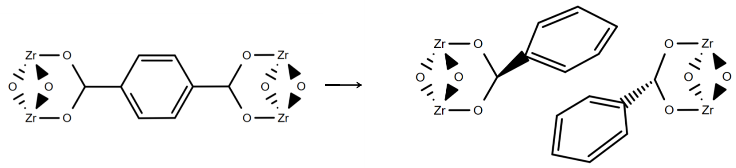

Figure 3.7.: A defect site created through benzoic acid.

For the nitrogen adsorption dataset, the predictors described in the previous section have been calculated using the pyGAPS framework (methods are described in chapter 1). The Henry constant is determined through the initial slope method, with a linear section found below 10^{-4} p/p_0. Total pore volume is taken as the liquid density of the amount adsorbed at 0.8 p/p_0, assuming that nitrogen is in a liquid-like state in the MOF pores. The pore size distribution was calculated through the Horvath-Kawazoe method for micropores, the Dollimore-Heal method for mesopores and DFT kernel fitting for a multiscale distribution. While the applicability of these methods for determination of absolute pore size of the UiO-66 framework may be put into question, they can be readily used to compare between different samples of the same material. In general, the leaching process has a positive effect on surface area and pore volume, both of which increase with a higher concentration of acid used. The strength of the initial interaction of the nitrogen probe with the pore walls is changed as well, with more defective samples likely to have a more pronounced interaction, either through the introduction of CUS or modification of pore environment.

The influence of the acid on the linker-to-node ratio appears to be constant throughout the solvents used, with an overall trend of TFA > FA > AA > BA. The order is similar to the acidic character of the compounds, except for benzoic acid which has a lower pKa (4.2) than acetic acid (4.7). The result is in accordance to the trend published by Shearer et al. when analysing the influence of these acids as used during modulated synthesis on the defectivity of the resulting material. [40]

When examining the influence of the solvent, another trend appears to emerge, with samples leached in DMSO having the largest propensity for defect generation, followed by DMF, water and methanol. In fact, a sample with a high concentration of TFA cannot be obtained, as the framework simply dissolves in the solution. The contribution of the of the solvent is not as easy to determine due to the complex interplay of multiple factors. The polarity of the solvent molecule has been linked to the rate of post synthetic ligand exchange from pristine UiO-66(Zr). [47] The leaching results do not, however, conform to the same trend, as water having a relative polarity of 1.0 introduces more defects than methanol (0.7) while DMF (0.38) is less effective than DMSO (0.44). The solubility of terephtalic acid in the solvent of choice may likely be a limiting factor driving its removal from the framework. Water, which has the

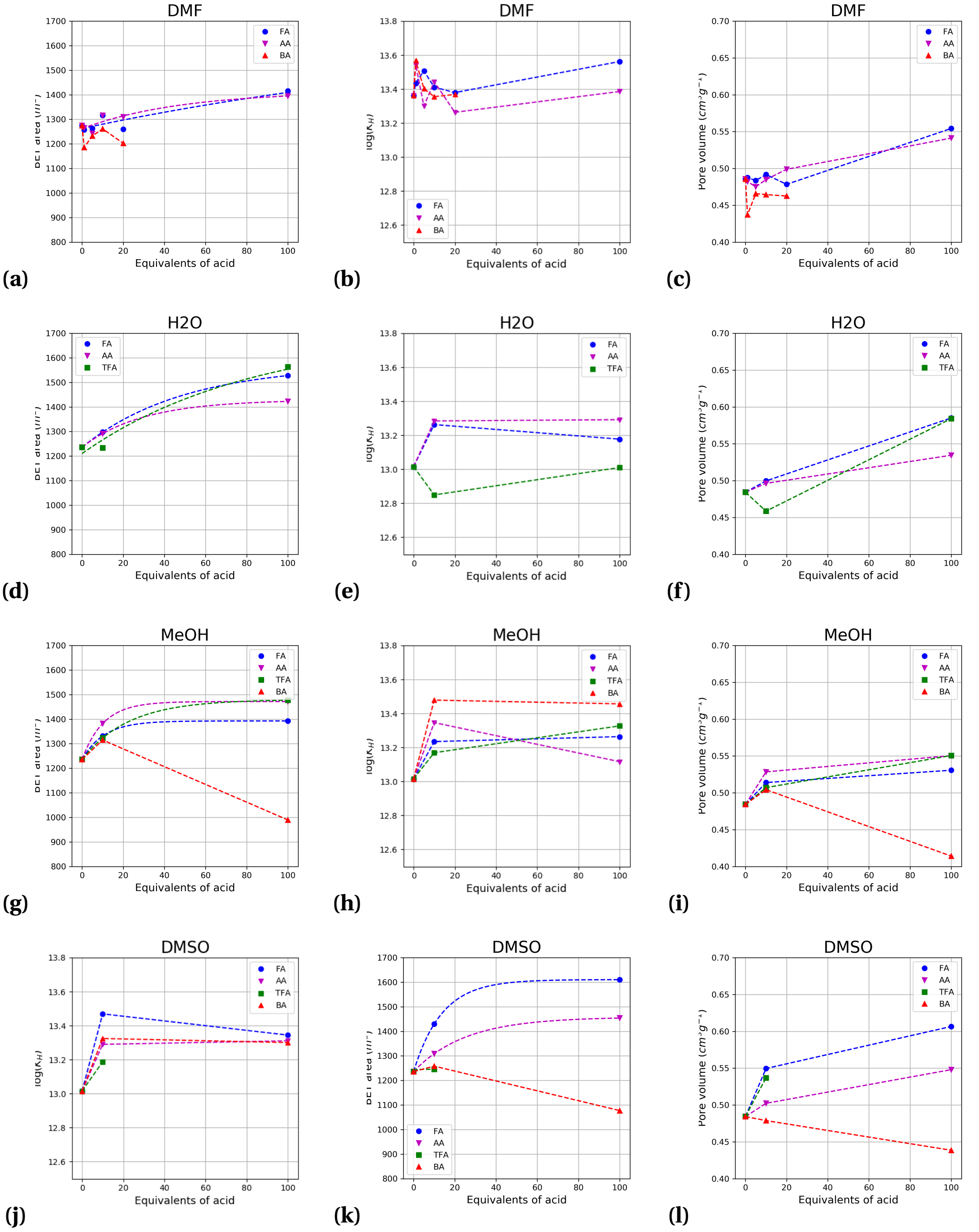

Figure 3.8.: Characterisation of all samples through predictors obtained through processing of the nitrogen physisorption data at 200 °C. The figure shows BET surface area (a-d), the logarithm of the initial Henry constant (e-h), and calculated pore volume (i-l) for DMF, H_2O, MeOH and DMSO leached materials, respectively.

lowest solubility for BTC, is one of the better solvents for defect generation, likely due to the high temperature of the reaction. As a strong acid is added, the equilibrium shifts even more towards the left, which may explain the worse performance of low equivalents of TFA in water as seen from adsorption predictors. At high concentrations, it is likely that the rate constant for the protonation of the metal-oxygen bond starts to dominate the leaching process. The viscosity of the solvent may also play a role in the mass transport of compounds through the porous media. However, the liquid with the highest kinematic viscosity, DMSO is actually the top performer during leaching, indicating that mass transfer may not be a factor.

The calculated pore sizes with both the HK method and the DFT method show two sharp peaks corresponding to the octahedral and tetrahedral pores in the UiO-66 structure. In Figure 3.9, the pore size distribution for the DMSO dataset is depicted, for both low temperature and high temperature activated variants. The appearance of a tertiary pore is visible in the leached samples with formic, acetic and trifluoroacetic acid. This pore size likely corresponds to the increased pore volume introduced by missing linker-type defects. The calculated diameter of this tertiary pore is inversely proportional to the molecular size of the leaching compound used, which is a clear indication of the presence of the acid molecules in the structure as capping agents. On the samples which have been activated to 320 °C, the pore width shifts to a single value as the coordinated acids are evacuated.

The pore size distribution calculated in the benzoic acid leached samples shows the disappearance of peaks larger than around 1 nm, as the compound replaces formate as the capping agent for the initial defects in the structure. Due to the similarity of the terephtalate linker with benzoate, the structure becomes more “ideal” than the pristine material. At high concentrations of benzoic acid, an overall decrease in porosity may be seen, as two benzoate molecules may act as capping agents in adjacent sites (Figure 3.7), effectively lowering the available pore volume. The effect is corroborated by trends in the linker-to-node ratio, surface area and total pore volume in both methanol, DMSO and to a lesser extent DMF.

At very high concentrations of TFA and BA, a fourth pore size begins to be appear in the DFT calculated pore distribution. This is likely evidence that missing cluster defects can be introduced at these concentrations. It should be noted that if such large-scale modifications of the structure are possible, complete structural breakdown is not far away. Indeed, samples with higher concentrations of acid could not be obtained with TFA in DMSO, with sample subjected to these conditions ending up completely dissolved. The appearance of this type of porosity in the samples treated with benzoic acid is counterintuitive, as the TGA linker ratio does not allude to any changes in coordination. In this case, it could be that missing cluster de-

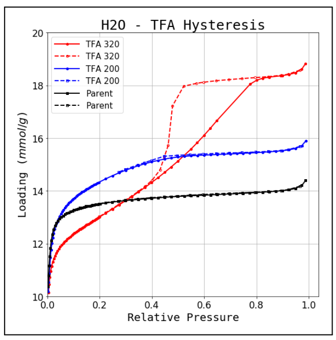

Figure 3.10.: Hysteresis loop in high temperature activated TFA treated UiO-66(Zr)

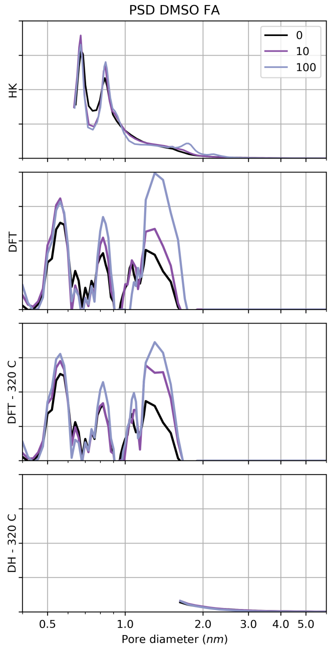

(a)

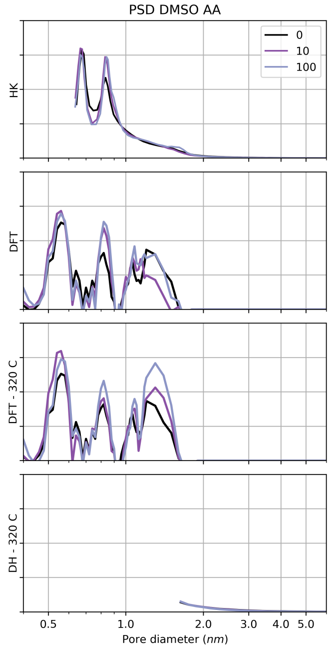

(b)

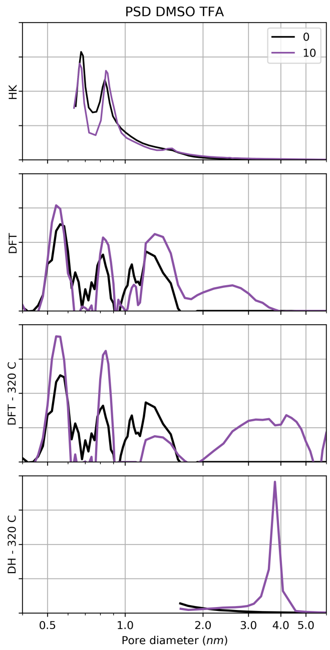

(c)

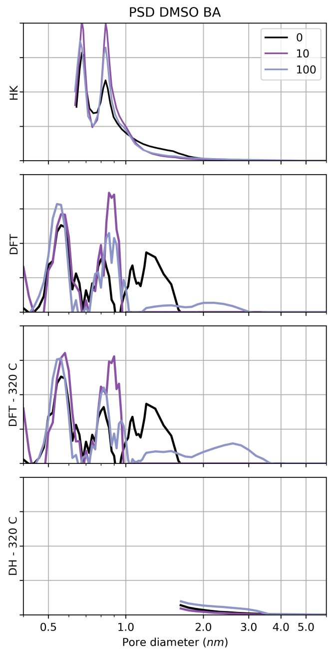

(d)

Figure 3.9.: Pore size distribution for the DMSO-leached samples as resulting from the HK (top), DFT (middle) and DH (bottom) methods on (a) formic acid, (b) acetic acid, (c) TFA and (d) BA. The top and bottom two distributions are calculated on the low and high temperature activated material respectively. The parent material is depicted in black.

fects are still generated forming a **reo**-benz phase [60] while the
excess of "dangling" benzoate moieties in the framework account for the decrease in surface area and capacity.

No hysteresis curve is observable on any samples activated at 200 °C. When activating at higher temperature, a hysteresis curve appears in the high concentration leached TFA samples (Figure 3.10), which corresponds to a pore size of around 4 nm in both DFT and DH calculated pore distribution. The shape of the hysteresis loop is also reminiscent of condensation in ink bottle-like pores, suggesting the existence of voids within the crystal matrix which are not directly accessible. This further confirms how effective highly acidic solutions can be at defect generation.

3.4.5. Carbon dioxide isotherms

The adsorption of carbon dioxide has been shown to be a good predictor for the presence of defects from comprehensive simulations by Thornton et al. [54]. In their work they have shown that in formate-capped defects, a shift of the CO_2 isotherm towards higher loading is seen at pressures over 5 bar, accompanied by a lower capacity at low pressures. Thus, in order to characterise the leached materials with a secondary probe molecule, carbon dioxide at 303 K was selected. Isotherms on the DMSO sample set are shown in Figure 3.11. The highest available acid ratio materials were selected, as the consequences of defects are likely to be more noticeable. Is should be noted that, since activation was performed at 200 °C, complete removal of some capping agents did not take place.

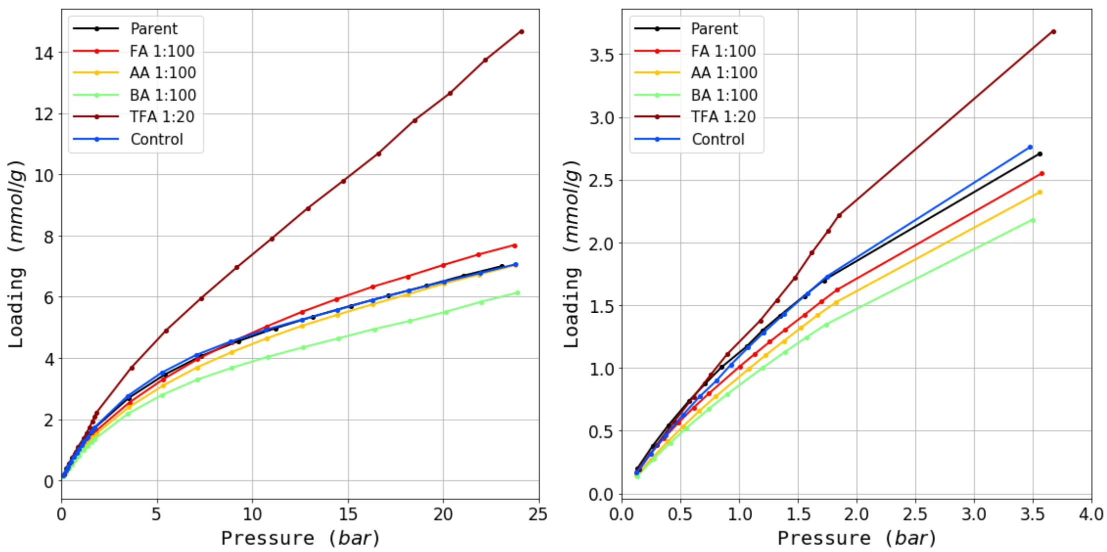

(a) **(b)**

Figure 3.11.: CO_2 adsorption isotherms at 303 K on different materials leached in DMSO in the (a) 0 bar to 25 bar range and the (b) 0 bar to 4 bar range. All materials were activated at 200 °C.

Isotherms follow similar trends as observed with nitrogen sorption and TGA analysis. A large increase in amount adsorbed can be seen on the TFA leached sample, with almost a doubling in the capacity at high pressure ranges. These values can only be obtained if a missing cluster *reo* net is the dominant phase of the material. Combined with the increased interactions with the framework at low loadings due to the fluorine moieties, this variant shows an astounding increase in adsorption capacity. The formate leached sample exhibits a cross-over of the parent material isotherm, highly similar to the simulated missing linker isotherms with around 11 linkers per metal node. A similar pattern may be present in the acetic acid isotherm, but with the intersection point at around 20 bar. The benzoic acid isotherm is shifted downwards throughout the entire pressure range, a further indication that this modulator has a counterproductive effect for obtaining defective materials through leaching. Finally, the control and parent materials have nearly identical isotherms, which confirms that the solvent does not act alone to generate defects in the structure.

3.5. Conclusion

In summary, a new method of generating missing linker and missing cluster type defects in a UiO-66(Zr) framework has been presented. This type of post-synthetic modification is an alternative to modulated synthesis, and can be useful when crystal growth is not desirable. It also introduces new possibilities of framework functionalisation, through sequential rounds of leaching and defect healing. It does, however, come at a cost, as it also partially dissolves the material.

A few trends emerge in regards to the capacity of different solvents and acids to induce defect formation.

- The impact of the monotopic acid is mainly due to its acidity, with pKa a being a good predictor of the resulting defectivity.
- DMSO and water stand out as the most effective solvents for defect generation.
- In general, the leached samples have a larger surface area and pore volume, due to both missing linker and cluster defects. Benzoic acid is a special case where due to its large molecule, may instead result in a loss of available pore space.
- High concentrations of acids may induce mesoporosity through large-scale defect generation. These conditions also make the material susceptible to complete structural breakdown through attack at the crystal surface.
- The resulting defective structures may have different bulk properties such as thermal and mechanical resistance due to the influence of the defect capping agents.
- The coordinated acids can also have an impact on the adsorption properties through changes to the pore environment.

These results also show the vast influence that defects have on the adsorption properties of MOFs. From different interactions with the material surface to vastly different capacities and, in some cases, even changing the sizes of pores or introducing new porosity. When attempting to determine the adsorption performance and behaviour of a compound it is important to consider whether the material in question is representative of its stoichiometric composition or, as is more often the case, a complex interplay of ideal and non-ideal domains.

Bibliography

[1] Robert E. Reed-Hill and R. Abbaschian. *Physical Metallurgy Principles*. The PWS-Kent series in engineering. PWS-Kent Pub, Boston, 3rd ed edition, 1992. ISBN 978-0-534-92173-6.

[2] Roland A. Levy and North Atlantic Treaty Organization, editors. *Microelectronic Materials and Processes: Proceedings of the NATO Aadvanced Study Institute on Microelectronic Materials and Processes, Il Ciocco, Castelvecchio Pascoli, Italy, June 30-July 11, 1986*. Number vol. 164 in NATO ASI series. Series E, Applied sciences. Kluwer Academic, Dordrecht ; Boston, 1989. ISBN 978-0-7923-0147-9 978-0-7923-0154-7.

[3] Anthony J. Leggett. What DO we know about high T c? *Nature Physics*, 2(3):134–136, March 2006. ISSN 1745-2473, 1745-2481. doi: 10.1038/nphys254.

[4] Yanzhong Pei, Heng Wang, and G. J. Snyder. Band Engineering of Thermoelectric Materials. *Advanced Materials*, 24(46):6125–6135, December 2012. ISSN 09359648. doi: 10.1002/adma.201202919.

[5] David S. Sholl and Ryan P. Lively. Defects in Metal–Organic Frameworks: Challenge or Opportunity? *The Journal of Physical Chemistry Letters*, 6(17):3437–3444, September 2015. ISSN 1948-7185. doi: 10.1021/acs.jpclett.5b01135.

[6] Jongwon Choi, Li-Chiang Lin, and Jeffrey C. Grossman. Role of Structural Defects in the Water Adsorption Properties of MOF-801. *The Journal of Physical Chemistry C*, 122(10):5545–5552, March 2018. ISSN 1932-7447, 1932-7455. doi: 10.1021/acs.jpcc.8b00014.

[7] Pritha Ghosh, Yamil J. Colón, and Randall Q. Snurr. Water adsorption in UiO-66: The importance of defects. *Chem. Commun.*, 50(77):11329–11331, 2014. ISSN 1359-7345, 1364-548X. doi: 10.1039/C4CC04945D.

[8] Jian-Rong Li, Ryan J Kuppler, and Hong-Cai Zhou. Selective gas adsorption and separation in metal–organic frameworks. *Chemical Society Reviews*, 38(5):1477, 2009. ISSN 0306-0012. doi: 10.1039/b802426j.

[9] Matthew J. Cliffe, Elizabeth Castillo-Martínez, Yue Wu, Jeongjae Lee, Alexander C. Forse, Francesca C. N. Firth, Peyman Z. Moghadam, David Fairen-Jimenez, Michael W. Gaultois, Joshua A. Hill, Oxana V. Magdysyuk, Ben Slater, Andrew L. Goodwin, and Clare P. Grey. Metal–Organic Nanosheets Formed via Defect-Mediated Transformation of a Hafnium Metal–Organic Framework. *Journal of the American Chemical Society*, 139(15):5397–5404, April 2017. ISSN 0002-7863, 1520-5126. doi: 10.1021/jacs.7b00106.

[10] Matthew J Cliffe, Wei Wan, Xiaodong Zou, Philip a Chater, Annette K Kleppe, Matthew G Tucker, Heribert Wilhelm, Nicholas P Funnell, François-Xavier Coudert, and Andrew L Goodwin. Correlated defect nanoregions in a metal-organic framework. *Nature communications*, 5(May):4176, 2014. ISSN 2041-1723. doi: 10.1038/ncomms5176.

[11] Thomas D. Bennett, Anthony K. Cheetham, Alain H. Fuchs, and François-Xavier Coudert. Interplay between defects, disorder and flexibility in metal-organic frameworks. *Nature Chemistry*, 9(1):11–16, December 2016. ISSN 1755-4330. doi: 10.1038/nchem.2691.

[12] Weibin Liang, Lin Li, Jingwei Hou, Nicholas D. Shepherd, Thomas D. Bennett, Deanna M. D'Alessandro, and Vicki Chen. Linking defects, hierarchical porosity generation and desalination performance in metal–organic frameworks. *Chemical Science*, 9(14):3508–3516, 2018. ISSN 2041-6520, 2041-6539. doi: 10.1039/C7SC05175A.

[13] Brandon J. Burnett, Paul M. Barron, and Wonyoung Choe. Recent advances in porphyrinic metal–organic frameworks: Materials design, synthetic strategies, and emerging applications. *CrystEngComm*, 14(11):3839, 2012. ISSN 1466-8033. doi: 10.1039/c2ce06692k.

[14] Mian Li, Dan Li, Michael O'Keeffe, and Omar M. Yaghi. Topological Analysis of Metal–Organic Frameworks with Polytopic Linkers and/or Multiple Building Units and the Minimal Transitivity Principle. *Chemical Reviews*, 114(2):1343–1370, January 2014. ISSN 0009-2665, 1520-6890. doi: 10.1021/cr400392k.

[15] Norbert Stock and Shyam Biswas. Synthesis of Metal-Organic Frameworks (MOFs): Routes to Various MOF Topologies, Morphologies, and Composites. *Chemical Reviews*, 112(2):933–969, February 2012. ISSN 0009-2665, 1520-6890. doi: 10.1021/cr200304e.

[16] Bart Bueken, Niels Van Velthoven, Andraž Krajnc, Simon Smolders, Francis Taulelle, Caroline Mellot-Draznieks, Gregor Mali, Thomas D. Bennett, and Dirk De Vos. Tackling the Defect Conundrum in UiO-66: A Mixed-Linker Approach to Engineering Missing Linker Defects. *Chemistry of Materials*, 29(24):10478–10486, December 2017. ISSN 0897-4756, 1520-5002. doi: 10.1021/acs.chemmater.7b04128.

[17] Amarajothi Dhakshinamoorthy, Abdullah M. Asiri, and Hermenegildo Garcia. Mixed-metal or mixed-linker metal organic frameworks as heterogeneous catalysts. *Catalysis Science & Technology*, 6(14):5238–5261, 2016. ISSN 2044-4753, 2044-4761. doi: 10.1039/C6CY00695G.

[18] Ji Woong Yoon, You-Kyong Seo, Young Kyu Hwang, Jong-San Chang, Hervé Leclerc, Stefan Wuttke, Philippe Bazin, Alexandre Vimont, Marco Daturi, Emily Bloch, Philip L. Llewellyn, Christian Serre, Patricia Horcajada, Jean-Marc Grenèche, Alirio E. Rodrigues, and Gérard Férey. Controlled Reducibility of a Metal-Organic Framework with Coordinatively Unsaturated Sites for Preferential Gas Sorption. *Angewandte Chemie International Edition*, 49(34):5949–5952, August 2010. ISSN 14337851. doi: 10.1002/anie.201001230.

[19] Kai Müller, Karin Fink, Ludger Schöttner, Meike Koenig, Lars Heinke, and Christof Wöll. Defects as Color Centers: The Apparent Color of Metal–Organic Frameworks Containing Cu 2+ -Based Paddle-Wheel Units. *ACS Applied Materials & Interfaces*, 9(42):37463–37467, October 2017. ISSN 1944-8244, 1944-8252. doi: 10.1021/acsami.7b12045.

[20] Paolo Falcaro, Raffaele Ricco, Amirali Yazdi, Inhar Imaz, Shuhei Furukawa, Daniel Maspoch, Rob Ameloot, Jack D. Evans, and Christian J. Doonan. Application of metal and metal oxide nanoparticles@MOFs. *Coordination Chemistry Reviews*, 307:237–254, January 2016. ISSN 00108545. doi: 10.1016/j.ccr.2015.08.002.

[21] Felicitas Schröder, Daniel Esken, Mirza Cokoja, Maurits W. E. van den Berg, Oleg I. Lebedev, Gustaaf Van Tendeloo, Bernadeta Walaszek, Gerd Buntkowsky, Hans-Heinrich Limbach, Bruno Chaudret, and Roland A. Fischer. Ruthenium Nanoparticles inside Porous [$Zn_4O(bdc)_3$] by Hydrogenolysis of Adsorbed [Ru(cod)(cot)]: A Solid-State Reference System for Surfactant-Stabilized Ruthenium Colloids. *Journal of the American Chemical Society*, 130(19):6119–6130, May 2008. ISSN 0002-7863, 1520-5126. doi: 10.1021/ja078231u.

[22] Gia-Thanh Vuong, Minh-Hao Pham, and Trong-On Do. Synthesis and engineering porosity of a mixed metal Fe_2Ni MIL-88B metal–organic framework. *Dalton Trans.*, 42(2):550–557, 2013. ISSN 1477-9226, 1477-9234. doi: 10.1039/C2DT32073H.

[23] Qingxia Yao, Jie Su, Ocean Cheung, Qingling Liu, Niklas Hedin, and Xiaodong Zou. Interpenetrated metal–organic frameworks and their uptake of CO2 at relatively low pressures. *Journal of Materials Chemistry*, 22(20):10345, 2012. ISSN 0959-9428, 1364-5501. doi: 10.1039/c2jm15933c.

[24] Ritesh Haldar, Nivedita Sikdar, and Tapas Kumar Maji. Interpenetration in coordination polymers: Structural diversities toward porous functional materials. *Materials Today*, 18(2):97–116, March 2015. ISSN 13697021. doi: 10.1016/j.mattod.2014.10.038.

[25] Rocio Semino, Naseem A. Ramsahye, Aziz Ghoufi, and Guillaume Maurin. Microscopic Model of the Metal–Organic Framework/Polymer Interface: A First Step toward Understanding the Compatibility in Mixed Matrix Membranes. *ACS Applied Materials & Interfaces*, 8(1):809–819, January 2016. ISSN 1944-8244, 1944-8252. doi: 10.1021/acsami.5b10150.

[26] Hartmut Gliemann and Christof Wöll. Epitaxially grown metal-organic frameworks. *Materials Today*, 15(3): 110–116, March 2012. ISSN 13697021. doi: 10.1016/S1369-7021(12)70046-9.

[27] Ivo Stassen, Nicholas Burtch, Alec Talin, Paolo Falcaro, Mark Allendorf, and Rob Ameloot. An updated roadmap for the integration of metal-organic frameworks with electronic devices and chemical sensors. *Chemical Society Reviews*, 46(11):3185–3241, 2017. ISSN 0306-0012. doi: 10.1039/C7CS00122C.

[28] Simon Krause, Volodymyr Bon, Irena Senkovska, Daniel M. Többens, Dirk Wallacher, Renjith S. Pillai, Guillaume Maurin, and Stefan Kaskel. The effect of crystallite size on pressure amplification in switchable porous solids. *Nature Communications*, 9(1), December 2018. ISSN 2041-1723. doi: 10.1038/s41467-018-03979-2.

[29] L. Vanduyfhuys, S. M. J. Rogge, J. Wieme, S. Vandenbrande, G. Maurin, M. Waroquier, and V. Van Speybroeck.

Thermodynamic insight into stimuli-responsive behaviour of soft porous crystals. *Nature Communications*, 9(1), December 2018. ISSN 2041-1723. doi: 10.1038/s41467-017-02666-y.

[30] Stefano Dissegna, Rifan Hardian, Konstantin Epp, Gregor Kieslich, Marie-Vanessa Coulet, Philip Llewellyn, and Roland A. Fischer. Using water adsorption measurements to access the chemistry of defects in the metal–organic framework UiO-66. *CrystEngComm*, pages 1–8, 2017. ISSN 1466-8033. doi: 10.1039/C7CE00224F.

[31] Chiara Caratelli, Julianna Hajek, Francisco G. Cirujano, Michel Waroquier, Francesc X. Llabrés i Xamena, and Veronique Van Speybroeck. Nature of active sites on UiO-66 and beneficial influence of water in the catalysis of Fischer esterification. *Journal of Catalysis*, 352:401–414, August 2017. ISSN 00219517. doi: 10.1016/j.jcat.2017.06.014.

[32] Thomas M. McDonald, Jarad A. Mason, Xueqian Kong, Eric D. Bloch, David Gygi, Alessandro Dani, Valentina Crocellà, Filippo Giordanino, Samuel O. Odoh, Walter S. Drisdell, Bess Vlaisavljevich, Allison L. Dzubak, Roberta Poloni, Sondre K. Schnell, Nora Planas, Kyuho Lee, Tod Pascal, Liwen F. Wan, David Prendergast, Jeffrey B. Neaton, Berend Smit, Jeffrey B. Kortright, Laura Gagliardi, Silvia Bordiga, Jeffrey A. Reimer, and Jeffrey R. Long. Cooperative insertion of CO2 in diamine-appended metal-organic frameworks. *Nature*, 519: 303, March 2015.

[33] Douglas A. Reed, Benjamin K. Keitz, Julia Oktawiec, Jarad A. Mason, Tomče Runčevski, Dianne J. Xiao, Lucy E. Darago, Valentina Crocellà, Silvia Bordiga, and Jeffrey R. Long. A spin transition mechanism for cooperative adsorption in metal–organic frameworks. *Nature*, September 2017. ISSN 0028-0836, 1476-4687. doi: 10.1038/nature23674.

[34] Nicholas C. Burtch, Himanshu Jasuja, and Krista S. Walton. Water Stability and Adsorption in Metal–Organic Frameworks. *Chemical Reviews*, 114(20):10575–10612, October 2014. ISSN 0009-2665, 1520-6890. doi: 10.1021/cr5002589.

[35] J. Raziel Álvarez, Elí Sánchez-González, Eric Pérez, Emilia Schneider-Revueltas, Ana Martínez, Adriana Tejeda-Cruz, Alejandro Islas-Jácome, Eduardo González-Zamora, and Ilich A. Ibarra. Structure stability of HKUST-1 towards water and ethanol and their effect on its CO $_2$ capture properties. *Dalton Transactions*, 46 (28):9192–9200, 2017. ISSN 1477-9226, 1477-9234. doi: 10.1039/C7DT01845B.

[36] Lei Shen, Shuo-Wang Yang, Shengchang Xiang, Tao Liu, Bangchuan Zhao, Man-Fai Ng, Jörg Göettlicher, Jiabao Yi, Sean Li, Lan Wang, Jun Ding, Banglin Chen, Su-Huai Wei, and Yuan Ping Feng. Origin of Long-Range Ferromagnetic Ordering in Metal–Organic Frameworks with Antiferromagnetic Dimeric-Cu(II) Building Units. *Journal of the American Chemical Society*, 134(41):17286–17290, October 2012. ISSN 0002-7863, 1520-5126. doi: 10.1021/ja3077654.

[37] Zhenlan Fang, Bart Bueken, Dirk E. De Vos, and Roland A. Fischer. Defect-Engineered Metal-Organic Frameworks. *Angewandte Chemie International Edition*, 54(25):7234–7254, June 2015. ISSN 14337851. doi: 10.1002/anie.201411540.

[38] Wenhua Zhang, Max Kauer, Olesia Halbherr, Konstantin Epp, Penghu Guo, Miguel I. Gonzalez, Dianne J. Xiao, Christian Wiktor, Francesc X. LIabrés i Xamena, Christof Wöll, Yuemin Wang, Martin Muhler, and Roland A. Fischer. Ruthenium Metal-Organic Frameworks with Different Defect Types: Influence on Porosity, Sorption, and Catalytic Properties. *Chemistry - A European Journal*, 22(40):14297–14307, September 2016. ISSN 09476539. doi: 10.1002/chem.201602641.

[39] Andreas Schaate, Pascal Roy, Adelheid Godt, Jann Lippke, Florian Waltz, Michael Wiebcke, and Peter Behrens. Modulated Synthesis of Zr-Based Metal-Organic Frameworks: From Nano to Single Crystals. *Chemistry - A European Journal*, 17(24):6643–6651, June 2011. ISSN 09476539. doi: 10.1002/chem.201003211.

[40] Greig C. Shearer, Sachin Chavan, Silvia Bordiga, Stian Svelle, Unni Olsbye, and Karl Petter Lillerud. Defect Engineering: Tuning the Porosity and Composition of the Metal-Organic Framework UiO-66 via Modulated Synthesis. *Chemistry of Materials*, 28(11):3749–3761, 2016. ISSN 15205002. doi: 10.1021/acs.chemmater.6b00602.

[41] Frederik Vermoortele, Rob Ameloot, Luc Alaerts, Roman Matthessen, Bert Carlier, Enrique V. Ramos Fernandez, Jorge Gascon, Freek Kapteijn, and Dirk E. De Vos. Tuning the catalytic performance of metal–organic frameworks in fine chemistry by active site engineering. *Journal of Materials Chemistry*, 22(20):10313, 2012. ISSN 0959-9428, 1364-5501. doi: 10.1039/c2jm16030g.

[42] Srinivas Gadipelli and Zhengxiao Guo. Postsynthesis Annealing of MOF-5 Remarkably Enhances the Framework Structural Stability and CO_2 Uptake. *Chemistry of Materials*, 26(22):6333–6338, November 2014. ISSN 0897-4756, 1520-5002. doi: 10.1021/cm502399q.

[43] Greig C. Shearer, Jenny G. Vitillo, Silvia Bordiga, Stian Svelle, Unni Olsbye, and Karl Petter Lillerud. Functionalizing the Defects: Postsynthetic Ligand Exchange in the Metal Organic Framework UiO-66. *Chemistry of Materials*, 28(20):7190–7193, October 2016. ISSN 0897-4756. doi: 10.1021/acs.chemmater.6b02749.

[44] Stephan Bernt, Vincent Guillerm, Christian Serre, and Norbert Stock. Direct covalent post-synthetic chemical modification of Cr-MIL-101 using nitrating acid. *Chemical Communications*, 47(10):2838, 2011. ISSN 1359-7345, 1364-548X. doi: 10.1039/c0cc04526h.

[45] Jasmina Hafizovic Cavka, Søren Jakobsen, Unni Olsbye, Nathalie Guillou, Carlo Lamberti, Silvia Bordiga, and Karl Petter Lillerud. A New Zirconium Inorganic Building Brick Forming Metal Organic Frameworks with Exceptional Stability. *Journal of the American Chemical Society*, 130(42):13850–13851, October 2008. ISSN 0002-7863. doi: 10.1021/ja8057953.

[46] Andrew D. Wiersum, Estelle Soubeyrand-Lenoir, Qingyuan Yang, Beatrice Moulin, Vincent Guillerm, Mouna Ben Yahia, Sandrine Bourrelly, Alexandre Vimont, Stuart Miller, Christelle Vagner, Marco Daturi, Guillaume Clet, Christian Serre, Guillaume Maurin, and Philip L. Llewellyn. An Evaluation of UiO-66 for Gas-Based Applications. *Chemistry - An Asian Journal*, 6(12):3270–3280, December 2011. ISSN 18614728. doi: 10.1002/asia.201100201.

[47] Min Kim, John F Cahill, Yongxuan Su, Kimberly A. Prather, and Seth M Cohen. Postsynthetic ligand exchange as a route to functionalization of 'inert' metal–organic frameworks. *Chem. Sci.*, 3(1):126–130, 2012. ISSN 2041-6520. doi: 10.1039/c1sc00394a.

[48] Lijuan Shen, Weiming Wu, Ruowen Liang, Rui Lin, and Ling Wu. Highly dispersed palladium nanoparticles anchored on UiO-66(NH2) metal-organic framework as a reusable and dual functional visible-light-driven photocatalyst. *Nanoscale*, 5(19):9374, 2013. ISSN 2040-3364, 2040-3372. doi: 10.1039/c3nr03153e.

[49] Sigurd Øien, Giovanni Agostini, Stian Svelle, Elisa Borfecchia, Kirill A. Lomachenko, Lorenzo Mino, Erik Gallo, Silvia Bordiga, Unni Olsbye, Karl Petter Lillerud, and Carlo Lamberti. Probing Reactive Platinum Sites in UiO-67 Zirconium Metal–Organic Frameworks. *Chemistry of Materials*, 27(3):1042–1056, February 2015. ISSN 0897-4756, 1520-5002. doi: 10.1021/cm504362j.

[50] Hui Wu, Yong Shen Chua, Vaiva Krungleviciute, Madhusudan Tyagi, Ping Chen, Taner Yildirim, and Wei Zhou. Unusual and highly tunable missing-linker defects in zirconium metal-organic framework UiO-66 and their important effects on gas adsorption. *Journal of the American Chemical Society*, 135(28):10525–10532, July 2013. ISSN 00027863. doi: 10.1021/ja404514r.

[51] Vincent Guillerm, Silvia Gross, Christian Serre, Thomas Devic, Matthias Bauer, and Gérard Férey. A zirconium methacrylate oxocluster as precursor for the low-temperature synthesis of porous zirconium(IV) dicarboxylates. *Chem. Commun.*, 46(5):767–769, 2010. ISSN 1359-7345, 1364-548X. doi: 10.1039/B914919H.

[52] Loredana Valenzano, Bartolomeo Civalleri, Sachin Chavan, Silvia Bordiga, Merete H. Nilsen, Søren Jakobsen, Karl Petter Lillerud, and Carlo Lamberti. Disclosing the Complex Structure of UiO-66 Metal Organic Framework: A Synergic Combination of Experiment and Theory. *Chemistry of Materials*, 23(7):1700–1718, April 2011. ISSN 0897-4756. doi: 10.1021/cm1022882.

[53] Marco Taddei, Russell Jon Wakeham, Athanasios Koutsianos, Enrico Andreoli, and Andrew Ross Barron. Post-synthetic ligand exchange in zirconium-based metal-organic frameworks: Beware of the defects! *Angewandte Chemie International Edition*, July 2018. ISSN 14337851. doi: 10.1002/anie.201806910.

[54] A. W. Thornton, R. Babarao, A. Jain, F. Trousselet, and F.-X. Coudert. Defects in metal–organic frameworks:

A compromise between adsorption and stability? *Dalton Trans.*, 45(10):4352–4359, 2016. ISSN 1477-9226, 1477-9234. doi: 10.1039/C5DT04330A.

[55] Frederik Vermoortele, Bart Bueken, Gaëlle Le Bars, Ben Van de Voorde, Matthias Vandichel, Kristof Houthoofd, Alexandre Vimont, Marco Daturi, Michel Waroquier, Veronique Van Speybroeck, Christine Kirschhock, and Dirk E. De Vos. Synthesis Modulation as a Tool To Increase the Catalytic Activity of Metal–Organic Frameworks: The Unique Case of UiO-66(Zr). *Journal of the American Chemical Society*, 135(31):11465–11468, August 2013. ISSN 0002-7863, 1520-5126. doi: 10.1021/ja405078u.

[56] Binbin Tu, Qingqing Pang, Doufeng Wu, Yuna Song, Linhong Weng, and Qiaowei Li. Ordered Vacancies and Their Chemistry in Metal–Organic Frameworks. *Journal of the American Chemical Society*, 136(41):14465–14471, October 2014. ISSN 0002-7863, 1520-5126. doi: 10.1021/ja5063423.

[57] Greig C. Shearer, Sachin Chavan, Jayashree Ethiraj, Jenny G. Vitillo, Stian Svelle, Unni Olsbye, Carlo Lamberti, Silvia Bordiga, and Karl Petter Lillerud. Tuned to Perfection: Ironing Out the Defects in Metal–Organic Framework UiO-66. *Chemistry of Materials*, 26(14):4068–4071, July 2014. ISSN 0897-4756, 1520-5002. doi: 10.1021/cm501859p.

[58] Yang Jiao, Yang Liu, Guanghui Zhu, Julian T. Hungerford, Souryadeep Bhattacharyya, Ryan P. Lively, David S. Sholl, and Krista S. Walton. Heat-Treatment of Defective UiO-66 from Modulated Synthesis: Adsorption and Stability Studies. *The Journal of Physical Chemistry C*, 121(42):23471–23479, October 2017. ISSN 1932-7447, 1932-7455. doi: 10.1021/acs.jpcc.7b07772.

[59] Ben Van de Voorde, Ivo Stassen, Bart Bueken, Frederik Vermoortele, Dirk De Vos, Rob Ameloot, Jin-Chong Tan, and Thomas D. Bennett. Improving the mechanical stability of zirconium-based metal–organic frameworks by incorporation of acidic modulators. *Journal of Materials Chemistry A*, 3(4):1737–1742, 2015. ISSN 2050-7488, 2050-7496. doi: 10.1039/C4TA06396A.

[60] Cesare Atzori, Greig C. Shearer, Lorenzo Maschio, Bartolomeo Civalleri, Francesca Bonino, Carlo Lamberti, Stian Svelle, Karl Petter Lillerud, and Silvia Bordiga. Effect of Benzoic Acid as a Modulator in the Structure of UiO-66: An Experimental and Computational Study. *The Journal of Physical Chemistry C*, 121(17):9312–9324, May 2017. ISSN 1932-7447, 1932-7455. doi: 10.1021/acs.jpcc.7b00483.

E. Appendix for chapter 3

E.1. Acid and solvent properties

Table E.1.: Solvent properties

Solvent	**Polarity** relative to water	**Boiling point** °C	**Viscosity** cP, at 20 °C	**Acidity** pKa
DMF	0.386	65	0.92	base of formic acid
DMSO	0.444	100	1.99	35
EtOH	0.762	153	0.54	15.5
H_2O	1.000	189	0.89	14

Table E.2.: Leaching acid properties

	Acidity	Solubility (g/100g) at 25 °C			
Acid	pKa	**H_2O**	**MeOH**	**DMF**	**DMSO**
formic	3.75	miscible	miscible	miscible	miscible
acetic	4.45	miscible	miscible	miscible	miscible
trifluoroacetic	0.3	miscible	miscible	miscible	miscible
benzoic	4.19	0.24 [(1)]	77 [(1)]	149 [(1)]	162 [(1)]

E.2. Powder diffraction patterns

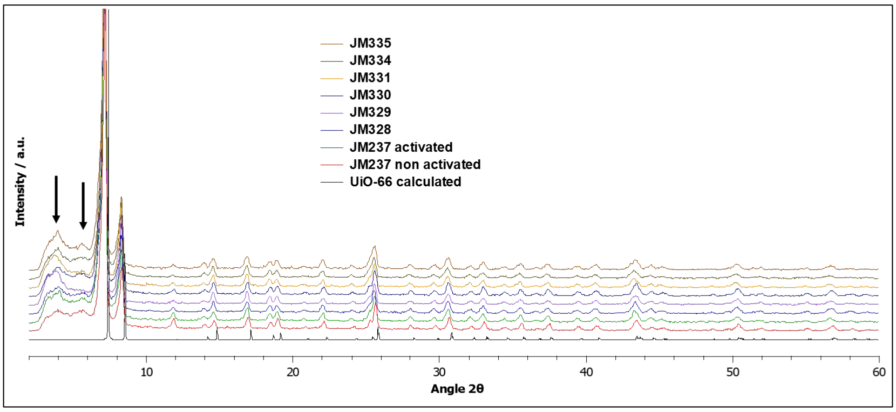

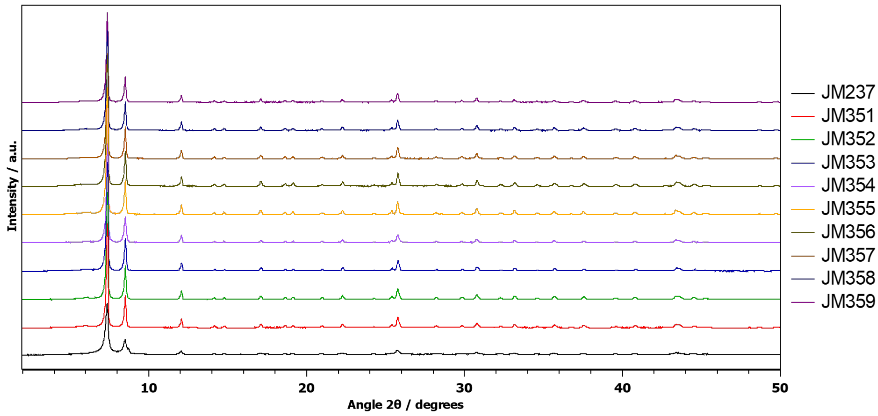

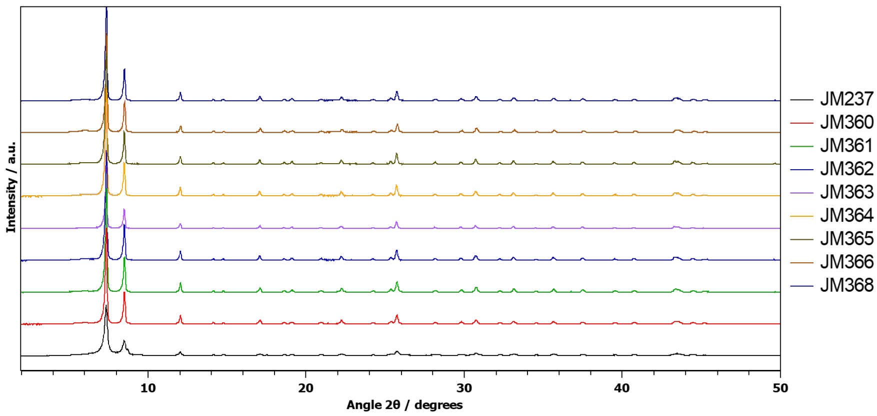

E.3. TGA curves

E.3.1. DMF leached samples

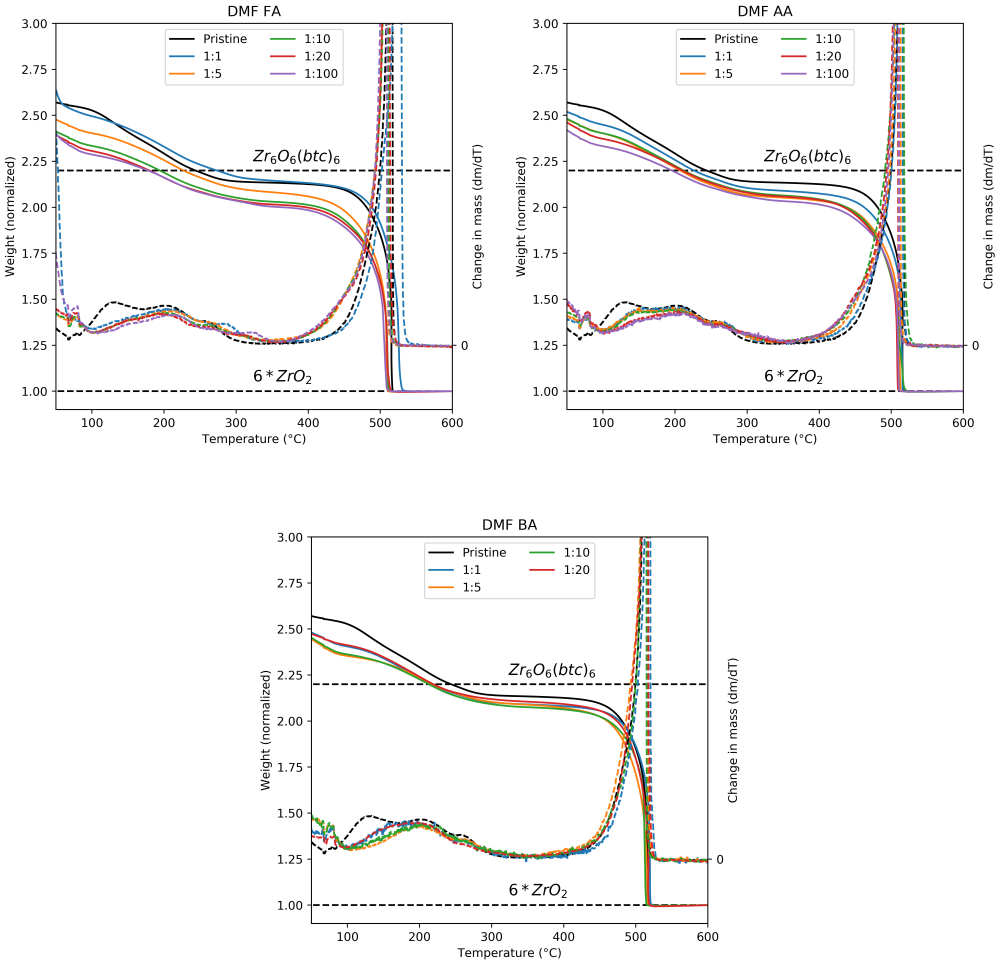

Figure E.1.: TGA curves for samples leached in DMF

E.3.2. Water leached samples

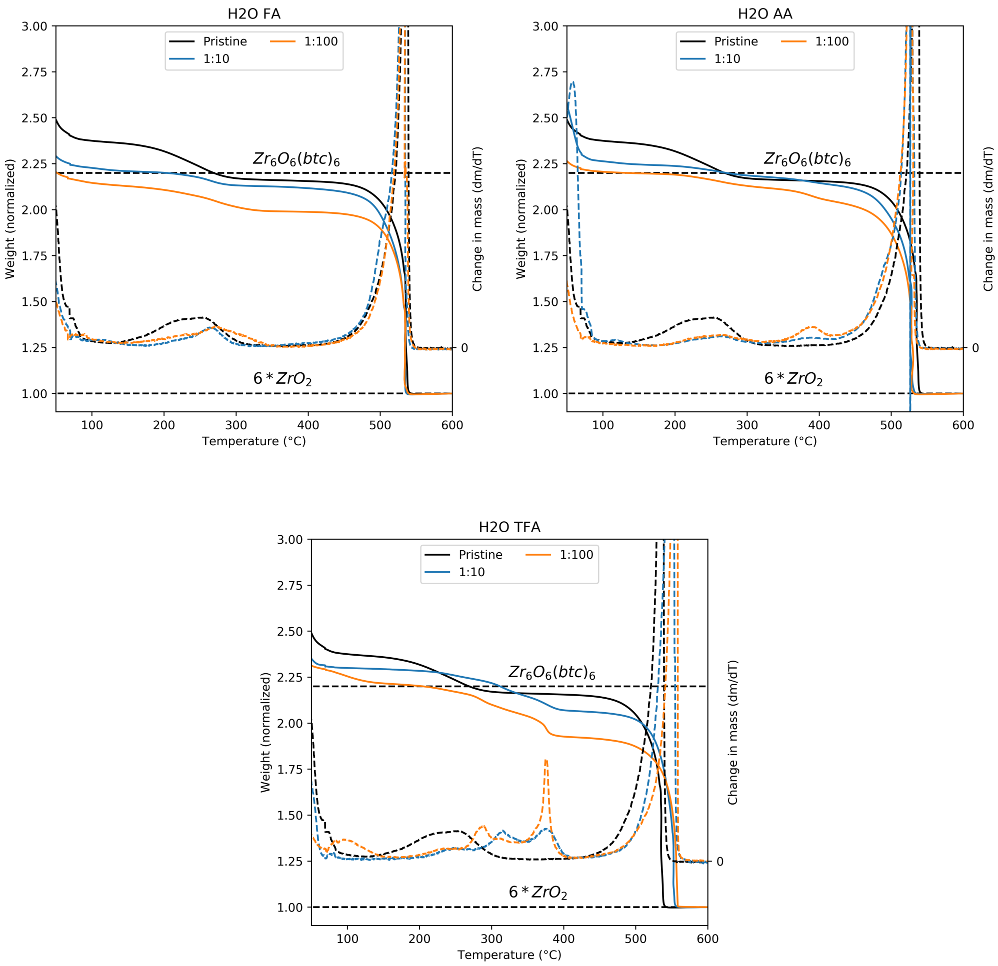

Figure E.2.: TGA curves for samples leached in H_2O

E.3.3. Methanol leached samples

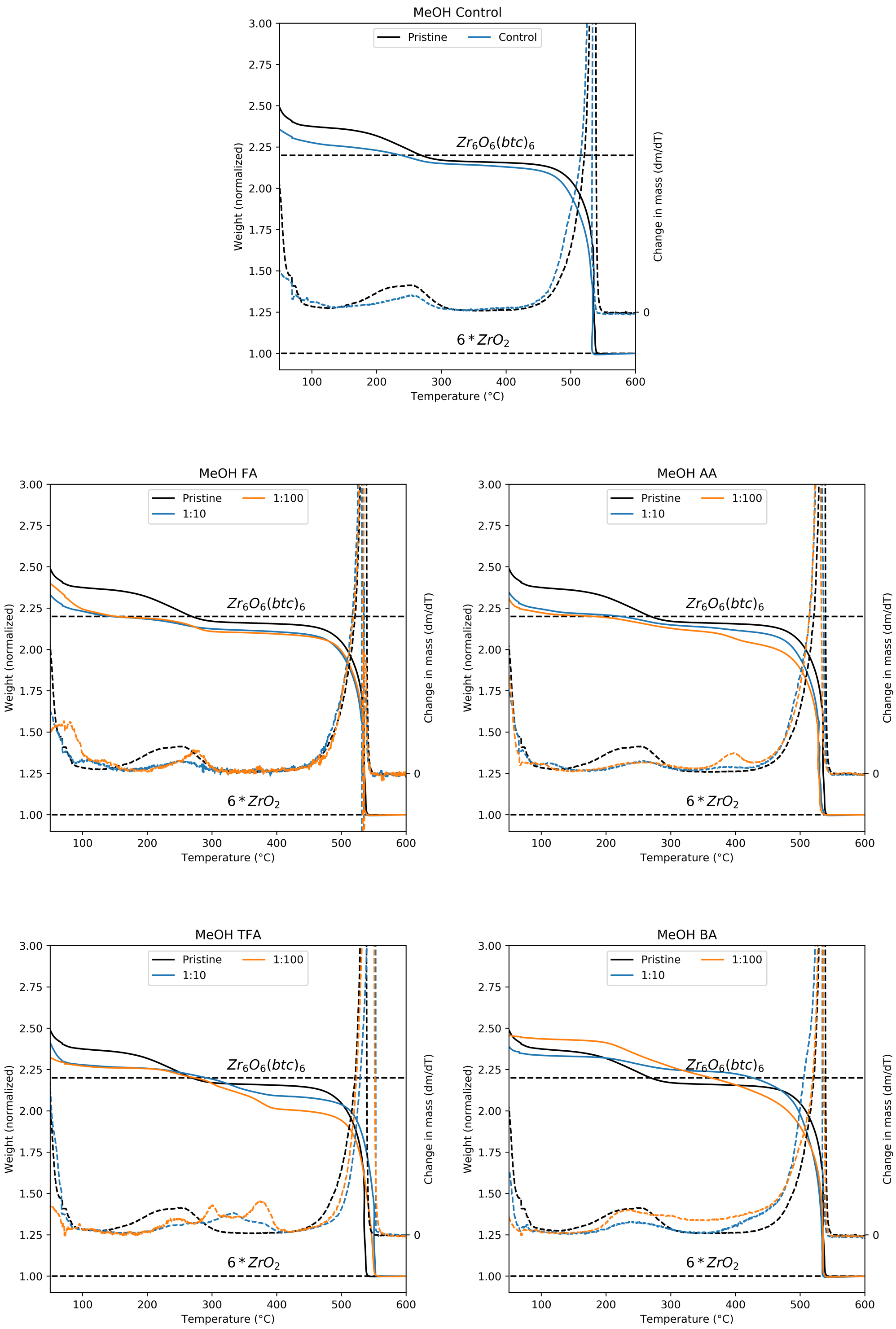

Figure E.3.: TGA curves for samples leached in MeOH

E.3.4. DMSO leached samples

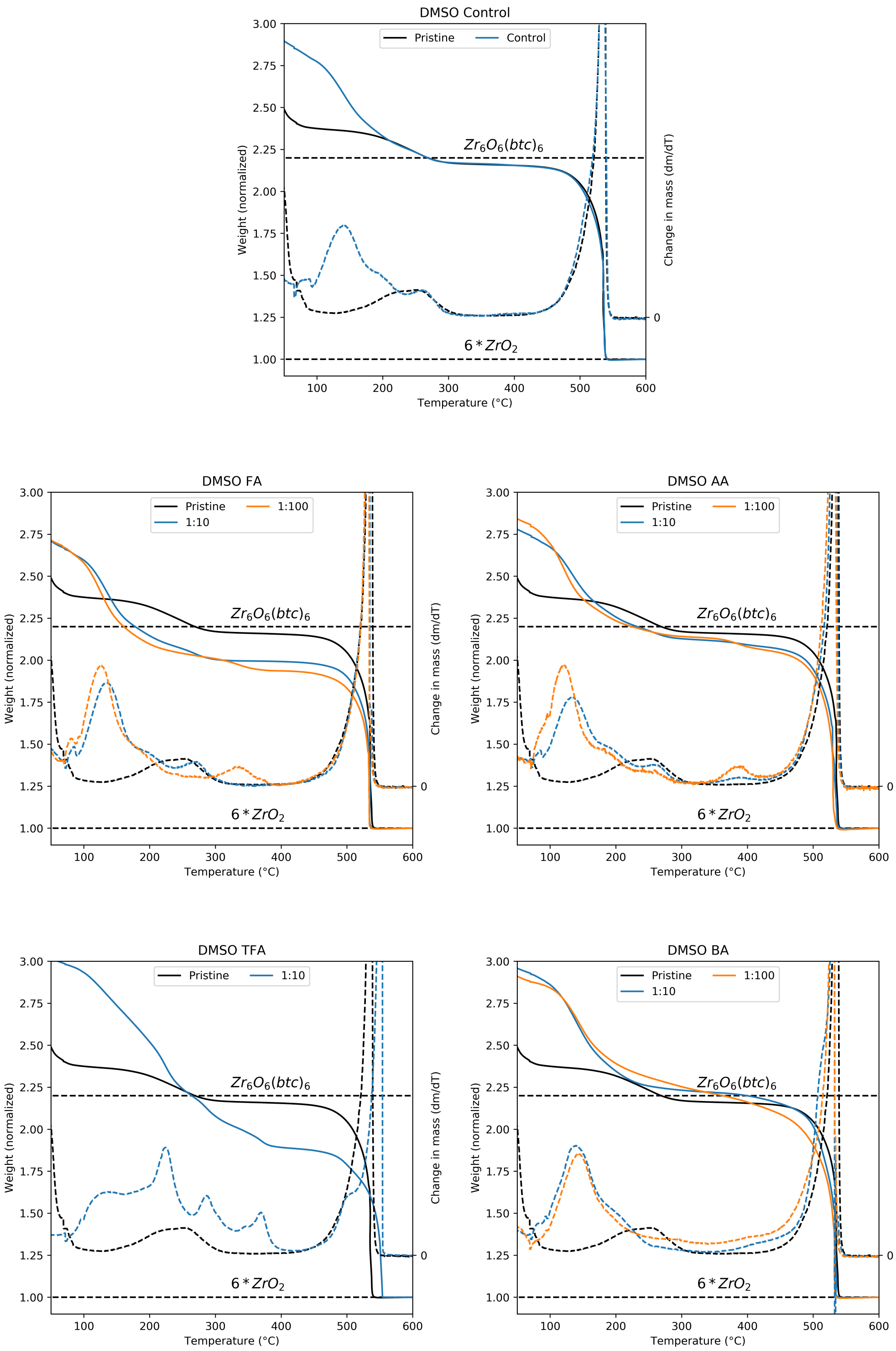

Figure E.4.: TGA curves for samples leached in DMSO

E.3.5. High resolution curves

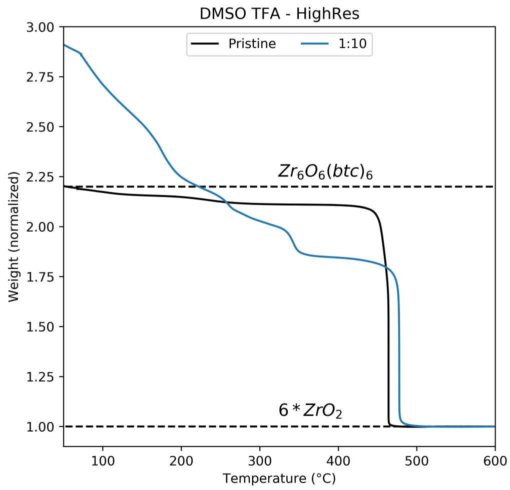

Figure E.5.: High resolution TGA curves for a DMSO/TFA leached sample

E.4. Nitrogen sorption isotherms

E.4.1. DMF leached samples

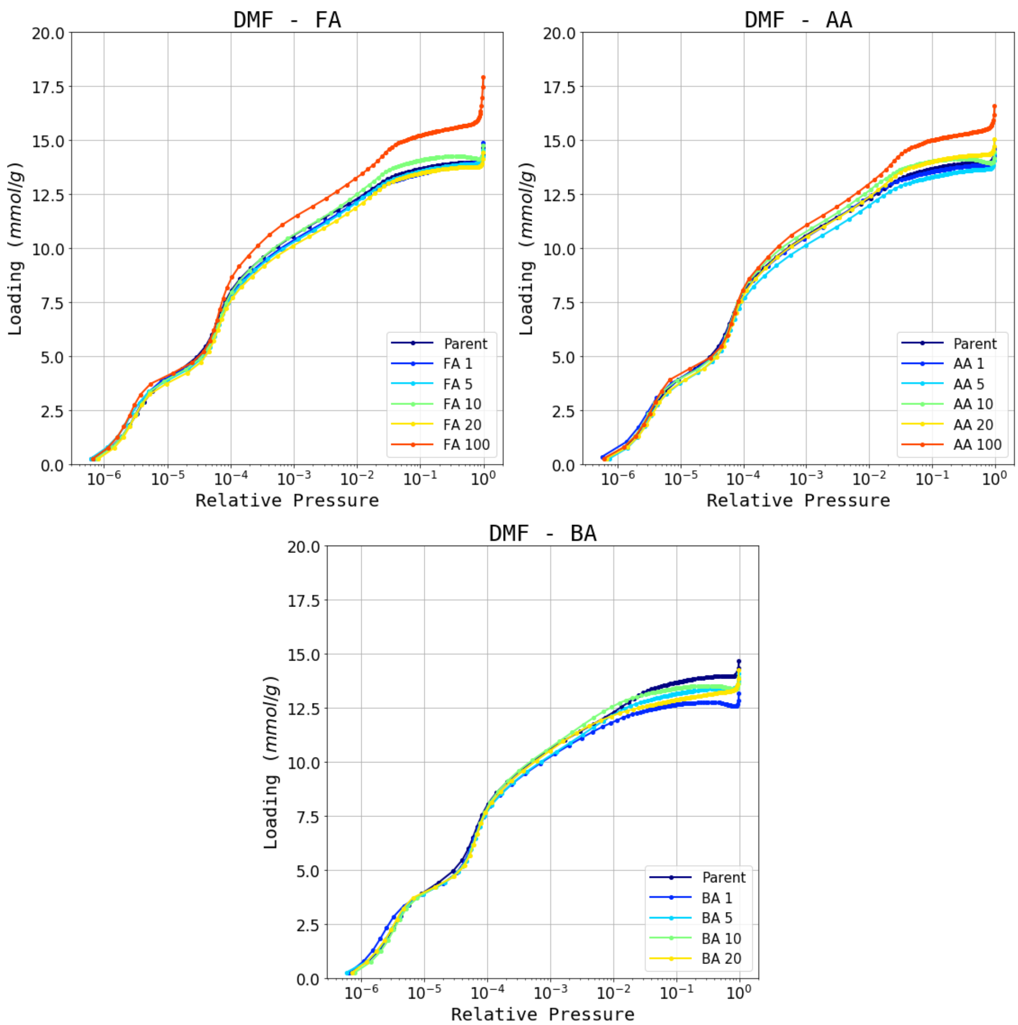

Figure E.6.: DMF isotherm dataset activated at 200 °C

E.4.2. H_2O leached samples

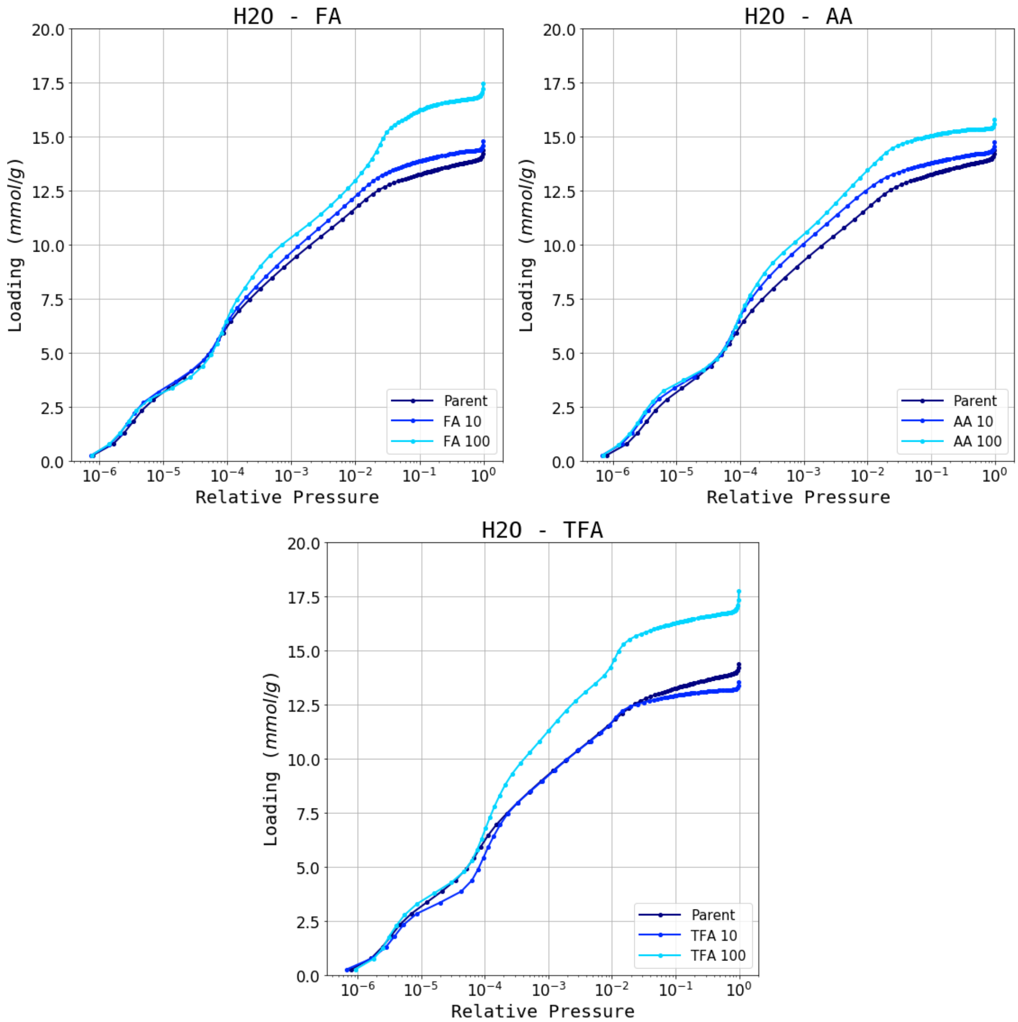

Figure E.7.: H_2O isotherm dataset activated at 200 °C

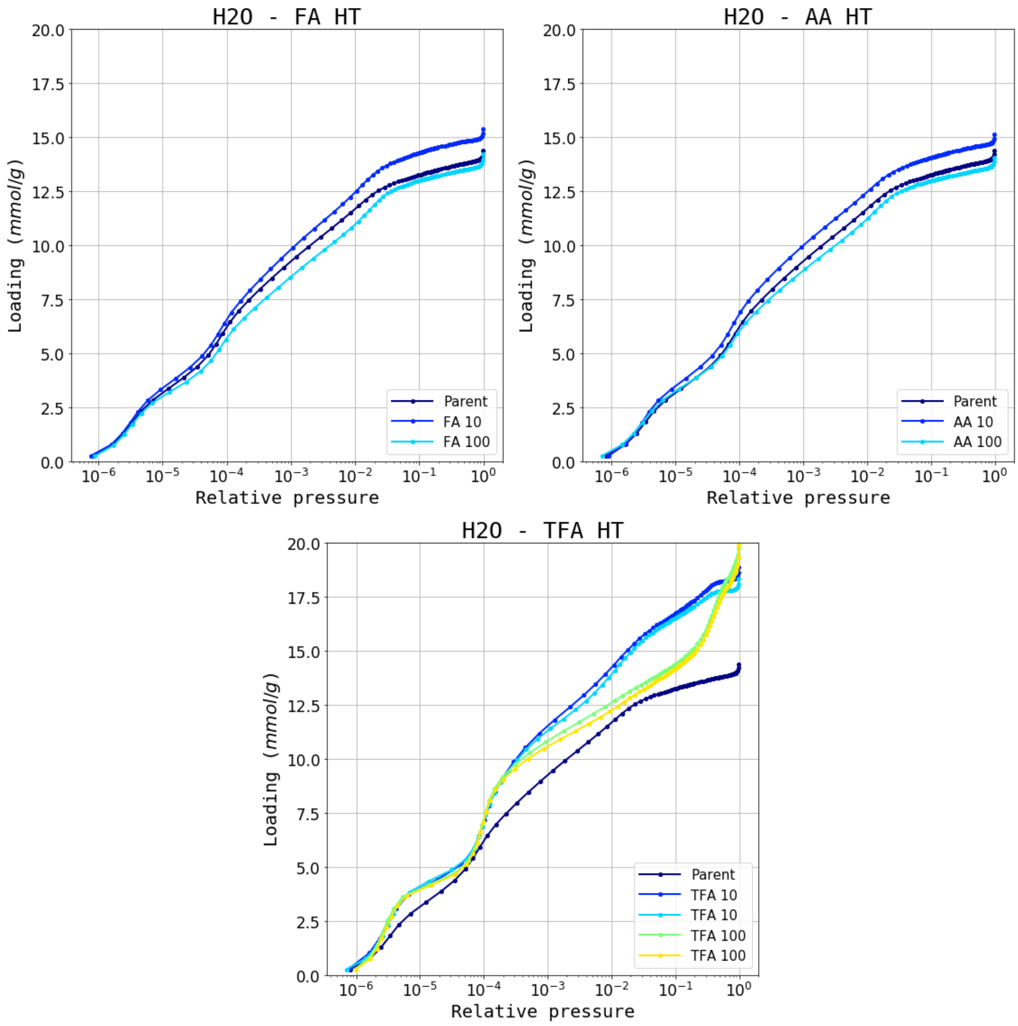

Figure E.8.: H_2O isotherm dataset activated at 320 °C

E.4.3. MeOH leached samples

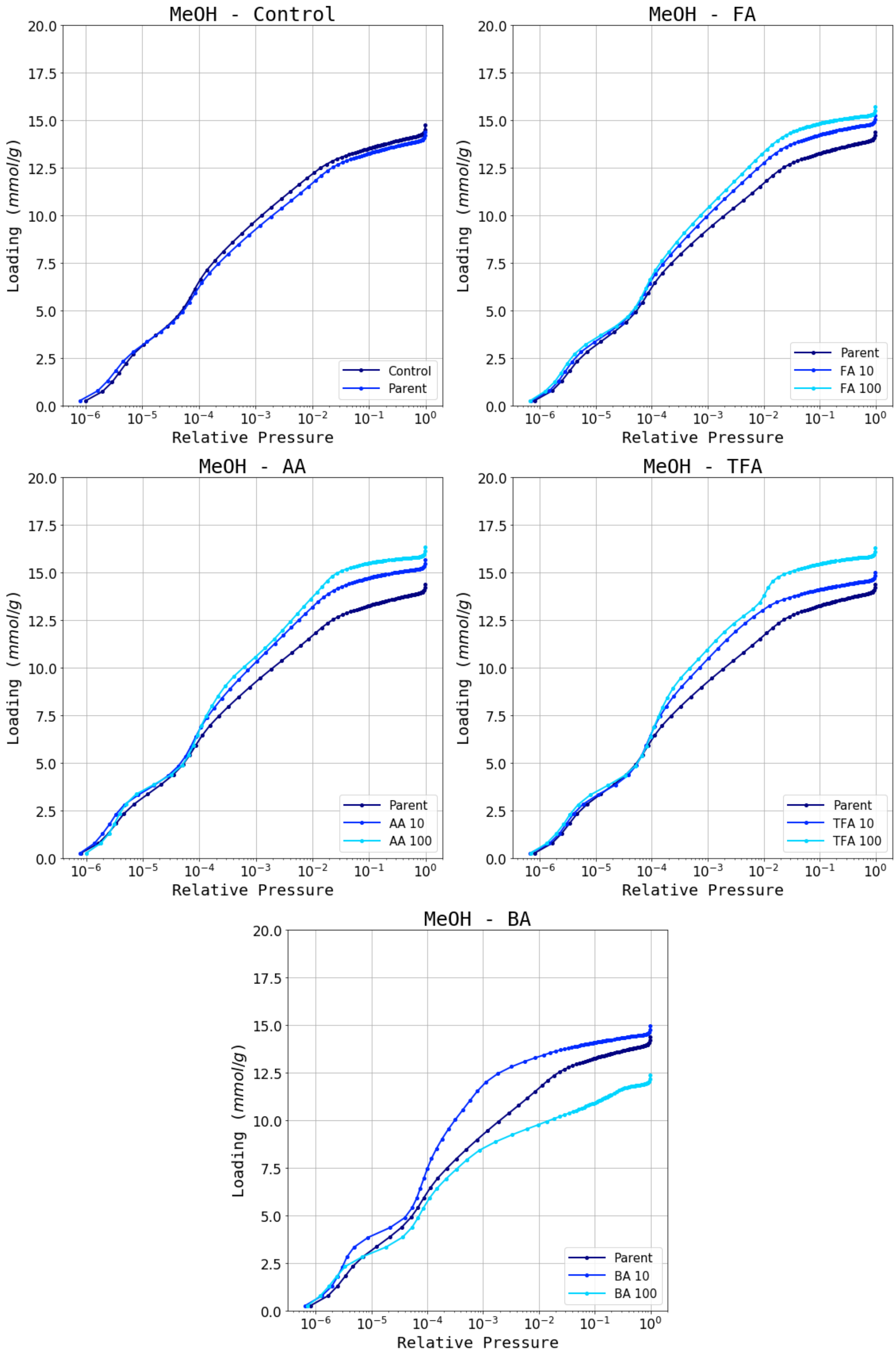

Figure E.9.: MeOH isotherm dataset activated at 200 °C

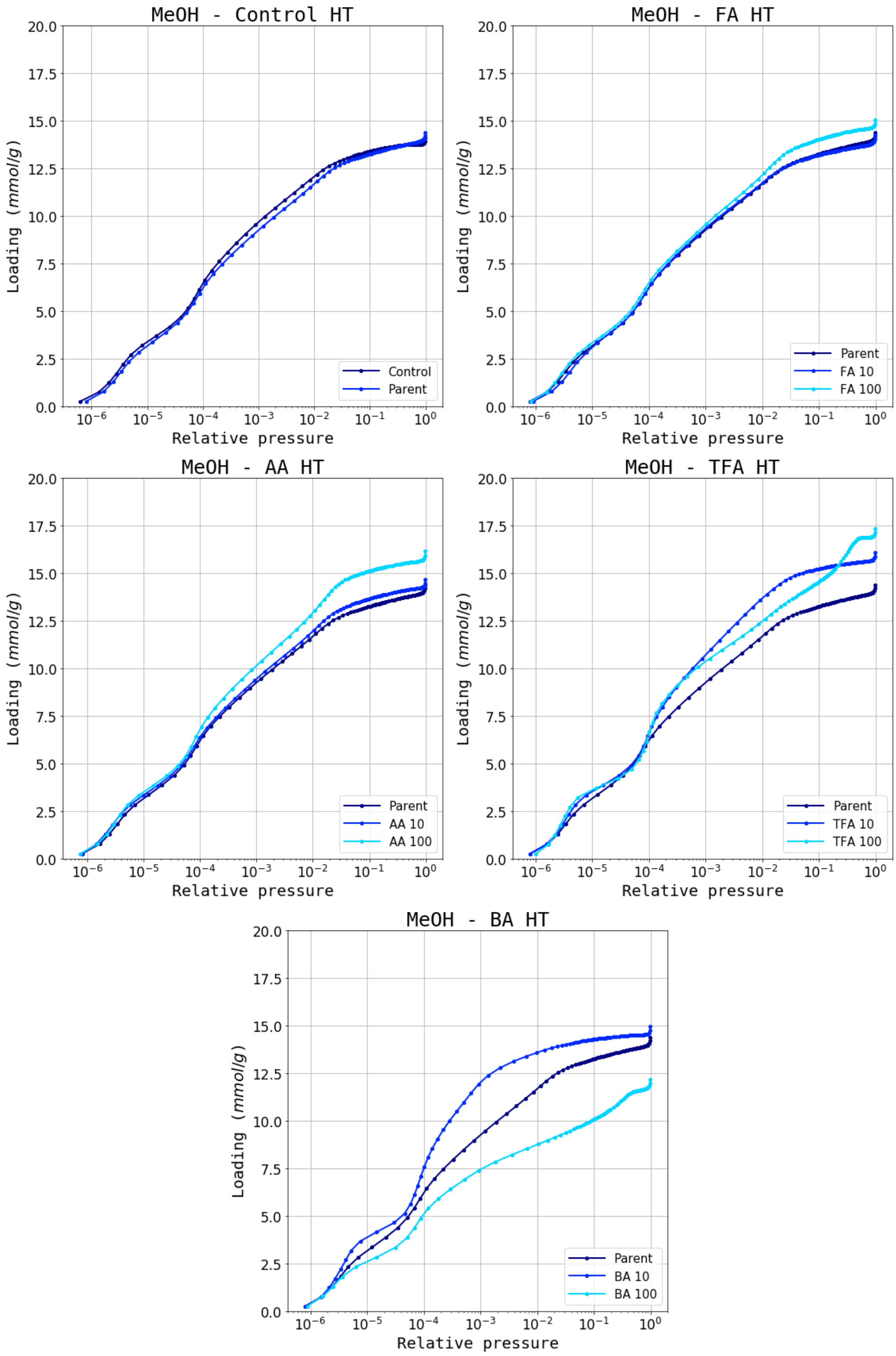

Figure E.10.: MeOH isotherm dataset activated at 320 °C

E.4.4. DMSO leached samples

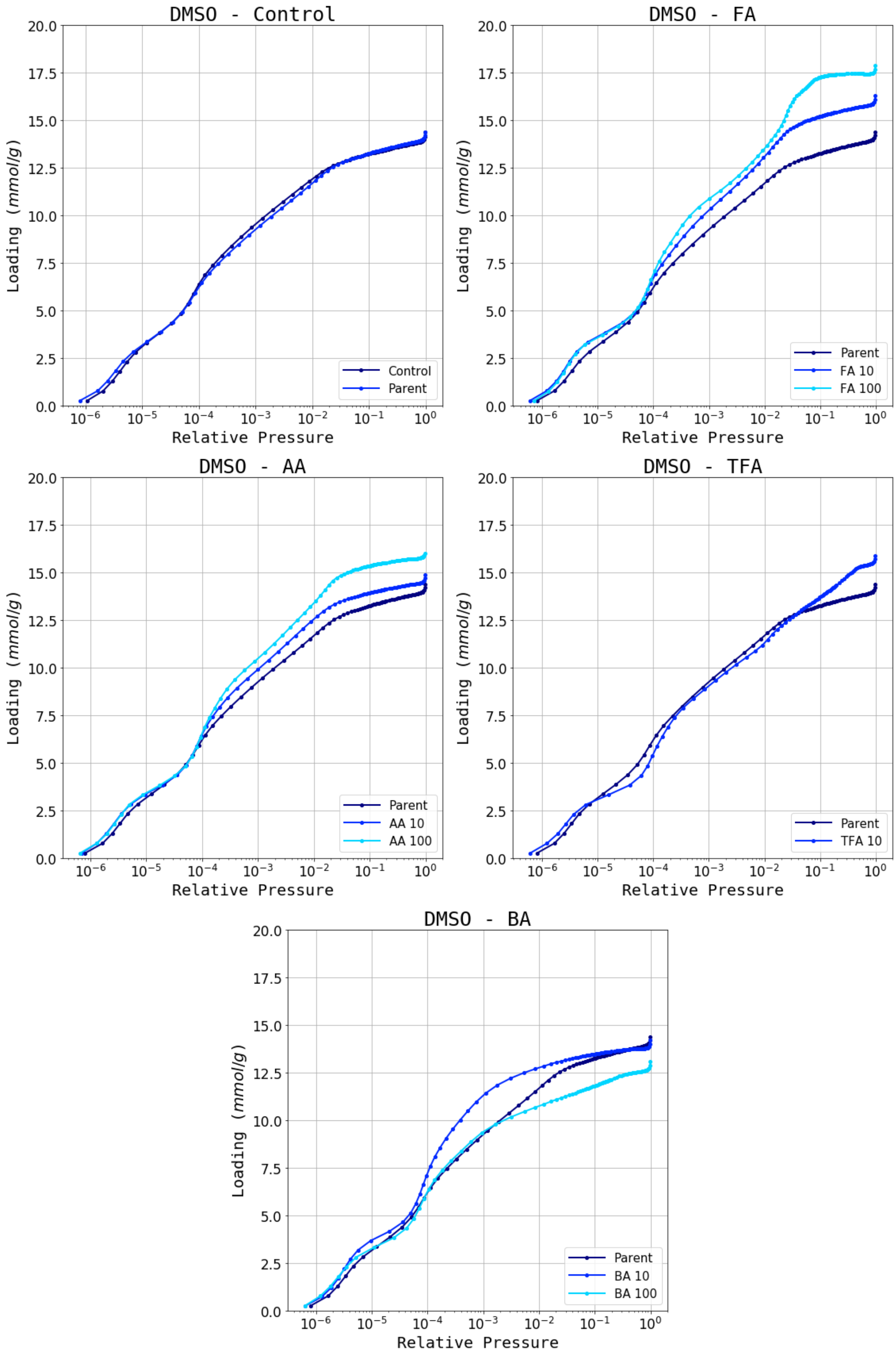

Figure E.11.: DMSO isotherm dataset activated at 200 °C

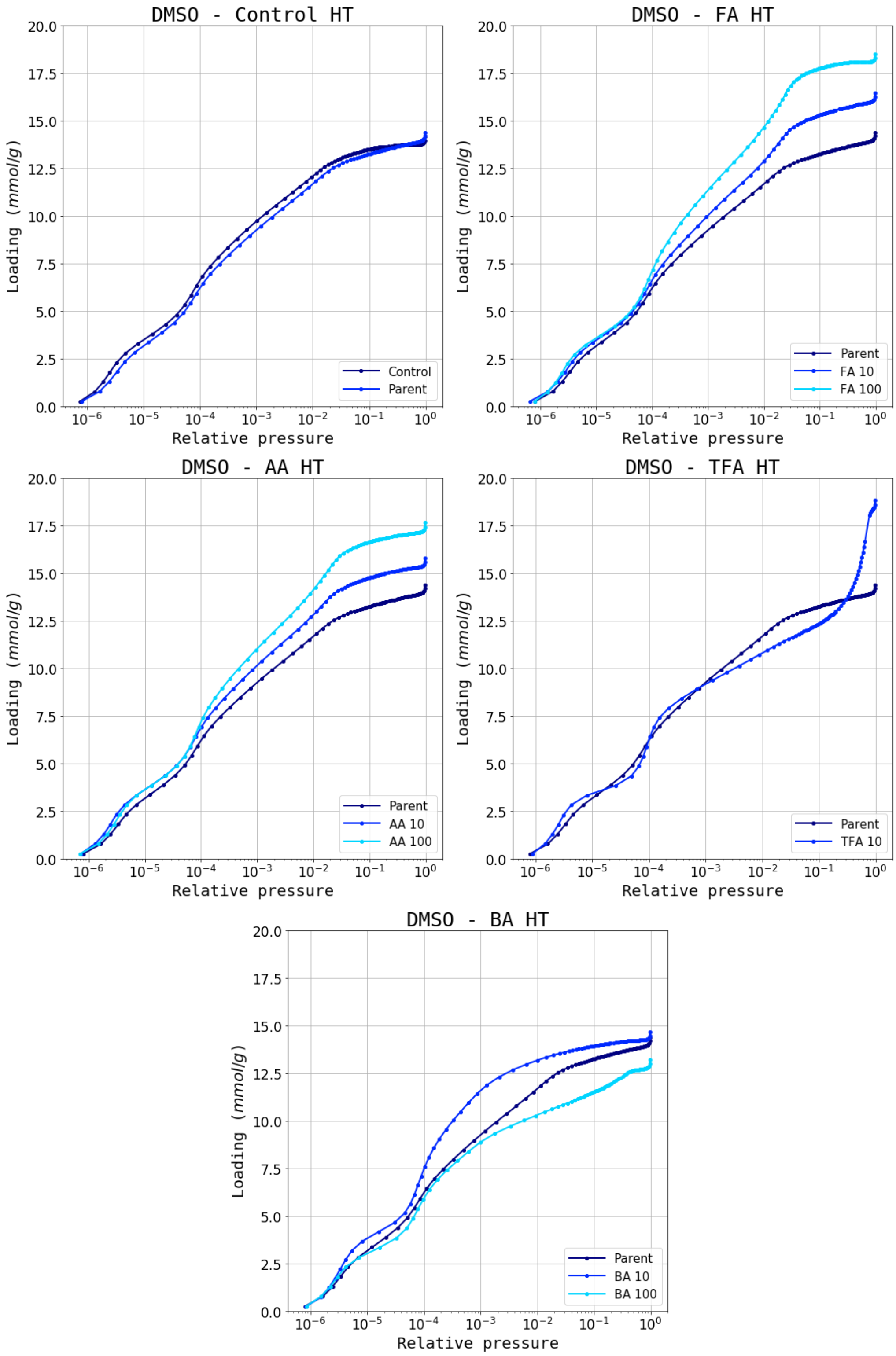

Figure E.12.: DMSO isotherm dataset activated at 320 °C

E.5. Characterisation

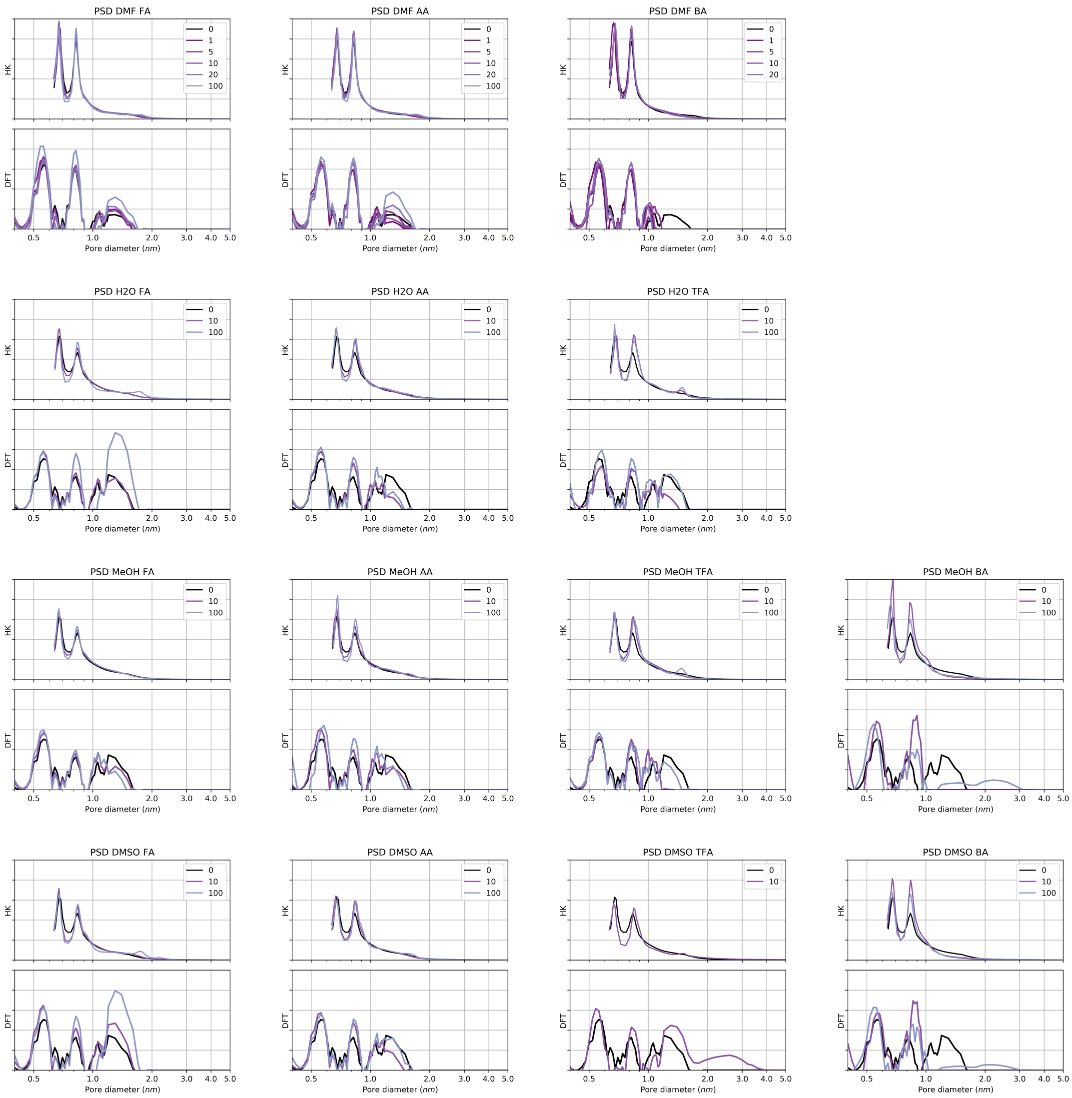

Bibliography

[1] William E. Acree. IUPAC-NIST Solubility Data Series. 99. Solubility of Benzoic Acid and Substituted Benzoic Acids in Both Neat Organic Solvents and Organic Solvent Mixtures. *Journal of Physical and Chemical Reference Data*, 42(3):033103, September 2013. ISSN 0047-2689, 1529-7845. doi: 10.1063/1.4816161.